AD-A019 632

LATERAL TRANSLATION OF EXPLOSION CRATER EJECTA: A WORKING MODEL BASED UPON PELLET EXPERIMENTS

Mark Settle

Air Force Cambridge Research Laboratories
Hanscom Air Force Base, Massachusetts

19 August 1975

DISTRIBUTED BY:

NTIS
National Technical Information Service
U. S. DEPARTMENT OF COMMERCE

027056

AD A019632

AFCRL-TR-75-0453
ENVIRONMENTAL RESEARCH PAPERS, NO. 528

Lateral Translation of Explosion Crater Ejecta: A Working Model Based Upon Pellet Experiments

MARK SETTLE, 1/LT, USAF

19 August 1975

Approved for public release; distribution unlimited.

TERRESTRIAL SCIENCES LABORATORY PROJECT 8607
AIR FORCE CAMBRIDGE RESEARCH LABORATORIES
HANSCOM AFB, MASSACHUSETTS 01731

AIR FORCE SYSTEMS COMMAND, USAF

Unclassified

SECURITY CLASSIFICATION OF THIS PAGE (When Data Entered)

REPORT DOCUMENTATION PAGE

READ INSTRUCTIONS BEFORE COMPLETING FORM

1. REPORT NUMBER: AFCRL-TR-75-0453	2. GOVT ACCESSION NO.
	3. RECIPIENT'S CATALOG NUMBER
4. TITLE (and Subtitle): LATERAL TRANSLATION OF EXPLOSION CRATER EJECTA: A WORKING MODEL BASED UPON PELLET EXPERIMENTS	5. TYPE OF REPORT & PERIOD COVERED: Scientific. Interim.
	6. PERFORMING ORG. REPORT NUMBER: ERP, No. 528
7. AUTHOR(s): Mark Settle, 1 Lt, USAF	8. CONTRACT OR GRANT NUMBER(s)
9. PERFORMING ORGANIZATION NAME AND ADDRESS: Air Force Cambridge Research Laboratories (LWW) Hanscom AFB Massachusetts 01731	10. PROGRAM ELEMENT, PROJECT, TASK AREA & WORK UNIT NUMBERS: 86070501 61102F
11. CONTROLLING OFFICE NAME AND ADDRESS: Air Force Cambridge Research Laboratories (LWW) Hanscom AFB Massachusetts 01731	12. REPORT DATE: 19 August 1975
	13. NUMBER OF PAGES: 6[illegible]
14. MONITORING AGENCY NAME & ADDRESS(if different from Controlling Office)	15. SECURITY CLASS. (of this report): Unclassified
	15a. DECLASSIFICATION/DOWNGRADING SCHEDULE

16. DISTRIBUTION STATEMENT (of this Report)

Approved for public release; distribution unlimited.

17. DISTRIBUTION STATEMENT (of the abstract entered in Block 20, if different from Report)

18. SUPPLEMENTARY NOTES

TECH, OTHER

19. KEY WORDS (Continue on reverse side if necessary and identify by block number)

Explosion cratering
Ejecta
Impact cratering

20. ABSTRACT (Continue on reverse side if necessary and identify by block number)

The excavation of explosion crater ejecta is a complex phenomenon in which the combined processes of stress-wave interaction and gas acceleration consistently transport successively deeper levels of the target or test medium to successively smaller ranges beyond the crater rim. A series of explosion experiments employing quartz sand and 1- to 10-lb explosive charges has been conducted in order to empirically describe the translation of artificial pellets emplaced within the test medium. The size and density of such pellets is

DD FORM 1 JAN 73 1473 EDITION OF 1 NOV 65 IS OBSOLETE

Unclassified

SECURITY CLASSIFICATION OF THIS PAGE (When Data Entered)

20. (Cont)

approximately comparable to the coarsest fraction of naturally occurring unconsolidated surficial materials (for example, playa and alluvium). A comparison of pellet throwout ranges with the translation of dyed sand and other artificial tracers in smaller and larger scale explosion experiments supports the analogy between the pellets employed here and the coarser size fraction of unconsolidated earth media.

The postshot range r of a mass point ejected by an explosive cratering event can be related to its preshot range x (measured from surface ground zero) by a power-law expression of the form: $(r/R) \propto (x/R)^c$, where absolute ranges x and r are normalized to R, the crater radius. Lateral (radial) translation of the artificial pellets ejected from the upper portions of the explosion craters could be approximately characterized by this expression with $c \cong -4.0 \pm 1.0$. In comparison, translation of the bulk of the ejecta excavated by larger explosion cratering experiments (for example, Stagecoach, Air Vent I) and smaller laboratory scale experiments (conducted at the University of Dayton Research Institute) in relatively unconsolidated earth media is characterized by the power law expression with $c \cong -2.5 \pm 1.0$. This relationship describing the lateral translation of the bulk of the ejecta is observed over a wide range of charge size and crater shape.

The lateral translation of the coarsest fraction of explosion crater ejecta initially situated near the original ground surface exceeds the average translation ranges of smaller particle sizes and thus poses the most severe natural missile hazard to personnel and surface facilities. The variation of the exponent c with depth within the crater of excavation for a series of experiments at various scaled depths of burst can be employed as an empirical model of the translation of the coarsest ejecta size fraction for larger scale explosion events.

A

Preface

Field assistance was provided by R. Dowling, D. Pendleton, SSgt R. Sands, and MSgt R. Tarnawa. The author is grateful for frequent discussions with S. Needleman. The coherence of the manuscript was improved considerably by the helpful comments of J.W. Head. The patience and effort of Cathy Dion in preparation of the manuscript is also appreciated.

Contents

Preceding page blank

Illustrations

Tables

Lateral Translation of Explosion Crater Ejecta: A Working Model Based Upon Pellet Experiments

1. INTRODUCTION

The ability to characterize the spatial and temporal distribution of ejecta produced by an explosive cratering event is essential to the development of accurate siting criteria for surface and near surface weapons systems and various support facilities (for example, detection and communication facilities). Empirical studies of block size distributions around explosion craters[1-3] together with ballistic models of ejection conditions[4,5] result in a partial, largely statistical description of the actual ejecta environment.[6] The ability to relate the process of ejecta deposition to the mechanics of excavation controlling the formation of the crater would contribute significantly to (1) developing a framework for extrapolating empirical ejecta studies to a variety of yields and geological settings, and (2) characterizing the relative threat the total ejecta environment poses to ground based facilities and personnel.

Similarly, the sampling goals of the recent Apollo missions have led to an intensive study of the impact cratering process.[7-11] Current theories describing the cratering of impact crater formation are based primarily upon (1) small scale impact experiments performed over a limited range of impact velocity, projectile size, and with idealized target materials, and (2) field relationships observed at

(Received for publication 19 August 1975)

*Due to the large number of references in above text, please refer to Reference Page No. 45 for references 1 through 11.

Preceding page blank

large terrestrial impact craters that have been preserved at various erosional levels. An impact cratering event in a layered target produces a stratified ejecta deposit with stratigraphy which is approximately inverted with respect to the local pre-existing layering, with deepest material deposited near the crater rim and successively shallower horizons extending to successively greater radial ranges. Geometrical models of ejecta distribution[10, 12] and secondary cratering effects[13, 14] have suggested that variations in the amount of primary ejecta and the velocity at which it impacts the original ground surface are responsible for the morphology of ejecta deposits observed over a range of impact crater size.[11, 15, 16] The variety of morphologies associated with impact crater ejecta deposits primarily reflects the range of particle velocity associated with the lateral translation of primary ejecta from the crater of excavation to a specific radial range. Generally, material thrown farther travels faster so that the total ejecta deposit can reflect a variety of depositional processes ranging from the low velocity overturning of massive sections of target material up onto the crater rim to a region of discontinuous secondary cratering at greater ranges (see Oberbeck, 1975).[11]

In comparison, the ejecta deposit produced by an explosive cratering event has qualitatively similar features: the deepest material excavated appears on or near the rim, and the ejecta deposit is thickest at the crater rim crest and thins rapidly at larger radial ranges. Oberbeck[17] has demonstrated dimensional similarities in crater shape and ejecta plume formation, and dynamic similarities in the radial attenuation of shock pressures for experimental impact and near-surface explosive cratering events. These similarities are observed for explosion craters with scaled depths of burst (SDOB) in the range 0.10 to 0.50 ft/(lb TNT)$^{1/3}$. This analogy between impact and near-surface explosion cratering may extend to much

12. McGetchin, T.R., Settle, M., and Head, J.W. (1973a) Radial thickness variation in impact crater ejecta: Implications for lunar basin deposits, Earth Planetary Sci. Lettr. 20:226-236.

13. Oberbeck, V.R., Morrison, R.H., Horz, F., Quaide, W.L., and Gault, D.E. (1974) Smooth Plains and Continuous Deposits of Craters and Basins, NASA Tech Mem X-62, 376, Ames Research Center, Moffett Field, California.

14. Oberbeck, V.R., Horz, F., Morrison, R.H., and Quaide, W.L. (1973) Emplacement of the Cayley Formation, NASA Tech Mem X-62, 302, Ames Research Center, Moffett Field, California.

15. Morrison, R.H., and Oberbeck, V.R. (1975) Features of crater continuous deposits and interpretations of their origin, Lunar Science VI, p. 578-580, The Lunar Science Institute, Houston, Texas.

16. Settle, M., and Head, J.W. (1975) Topographic variations in lunar crater rim profiles: Implications for the formation of ejecta deposits, submitted to Icarus.

17. Oberbeck, V.R. (1971) Laboratory simulation of impact cratering with high explosives, Jour. Geophys. Res. 76:5732-5749.

larger craters.[18] Thus, the variety of depositional processes which characterize large impact craters may also be produced by correspondingly large, near-surface explosive events. In fact, an annular zone of secondary craters was produced by the Sedan explosion, a large nuclear explosion in alluvium.[19]

1.1 Purpose of the Present Study

A complete characterization of the mechanics of ejecta deposition should include a description of ejection velocity, ejection angle, particle size distribution, and postshock strength of material excavated by an individual cratering event. These ejection parameters are primarily determined by the response of the specific material to the stress wave generated by both explosive and impact events and by the acceleration of gases produced in the explosion case. The postshock strength of the material, ejecta particle size distributions, and ejection parameters generally reflect the relative intensity of the stress wave at different distances from the center of the crater. The subsequent excavation stage of the crater formation process then redistributes these stress-induced variations by translating material to a variety of ranges. The distribution and morphology of the resulting ejecta deposit represent a transformed record of excavation parameters within the transient crater of excavation during the cratering event.

The purpose of the present study is to empirically characterize the 'transformation function' by which the excavation phase of an explosive cratering event translates material from a pre-event position to a post-event range within the ejecta deposit. The relationship between the original and final position of ejected material places important constraints on the distribution of shock stress and kinetic energy produced within the test medium by the explosion. This, in turn, permits the association of observed ejecta morphologies such as the hummocky and grooved terrain observed within the continuous ejecta deposit, ejecta rays, and discontinuous ejecta clusters with the relative levels of energy distribution within the test medium.

The explosion cratering experiments described in this report were designed to empirically describe the material translation process. Tracer pellets were emplaced at specific positions within the test medium prior to a shot, then these pellets were located and their final positions were surveyed after the shot. Lateral pellet translation refers to the radial displacement of a pellet produced by the explosive cratering event measured from surface ground zero (SGZ). All experiments

18. Baldwin, R. B. (1963) The Measure of the Moon, The University of Chicago Press, Chicago, Illinois.

19. Roberts, W. A. (1965) Permanent angular displacement and ejecta-induced impulse associated with crater formation, Icarus 4:480-493.

were conducted at SDOB in the range appropriate to the impact crater analogy. Thus, the results of the present study can be directly compared with small impact cratering experiments.

2. THE EXPERIMENTS: SETTING, MATERIALS, AND PROCEDURE

Small scale explosive cratering experiments were conducted within the Ft. Devens Reservation during the period of September 1973 through September 1974. The pellet experiments described in this report represent a part of the total research program accomplished during this period. The results of parallel studies concerning the effects of explosive cratering on the bearing strength of granular earth materials will be reported elsewhere (see Settle and Needleman (1974) for preliminary results[20]).

2.1 Test Site

All cratering experiments were performed in an area approximately 50 m × 75 m within the Hotel Range on the Ft. Devens Reservation (see Figure 1). The bedrock geology of the area consists of a metamorphosed sequence of carboniferous sedimentary units situated within the Worcester trough. In the vicinity of the test site, this sequence is represented by phyllite, schist, and quartzite rocks which are extensively intruded by granite and minor amounts of diabase.[21] The surface geology surrounding the site is dominated by glacial deposits of variable thickness.

Hotel Range in particular is an area of substantial fill, consisting mostly of quartz sand with minor amounts (< 3 percent) of feldspar and mica also present. Seismic investigation of the subsurface structure of the site has revealed that the deposit of fill extends to a depth of approximately 2 to 3 m and has an acoustic velocity of 1000 m/sec. The fill rests upon much coarser material which appears to be a deposit of glacial till (S. Needleman, personal communication).

The edges of Hotel Range are generally overgrown with bushes and saplings while the periphery of the actual test site is consolidated primarily by grasses and mosses (see Figure 1). The range of particle size distributions of the

20. Settle, M., and Needleman, S. (1974) Deformation in granular earth media produced by explosive cratering: Implications for impact cratering, EOS Transactions Am. Geophys. Union 56, No. 12:1142.

21. Emerson, B.K. (1917) Geology of Massachusetts and Rhode Island, U.S. Geological Survey Bull. No. 597, 289 pp.

Figure 1. Sketch Map of Hotel Range on the Fort Devens Reservation. Explosion experiments reported in this paper were conducted within the sand fill area

unconsolidated quartz sand fill near the surface of the test site is shown in Figure 2. Generally 10 percent of the surface material is coarser than 1 mm while approximately 50 percent of the surface material is finer than 0.5 mm. Repeated precipitation in areas of fill will commonly wash finer material from the near surface portion of the fill deposit and redeposit this finer material at greater depth. Such an effect has been observed at the Boeing Company Tulalip test site.[24] Indeed, grain size analysis of subsurface samples reveals that a shallow ledge of finer, clay-like material exists approximately 0.5 m beneath the western side of the test site. This is consistent with the drainage of the area: the test site dips gently to the south southwest by 3° to 5°.

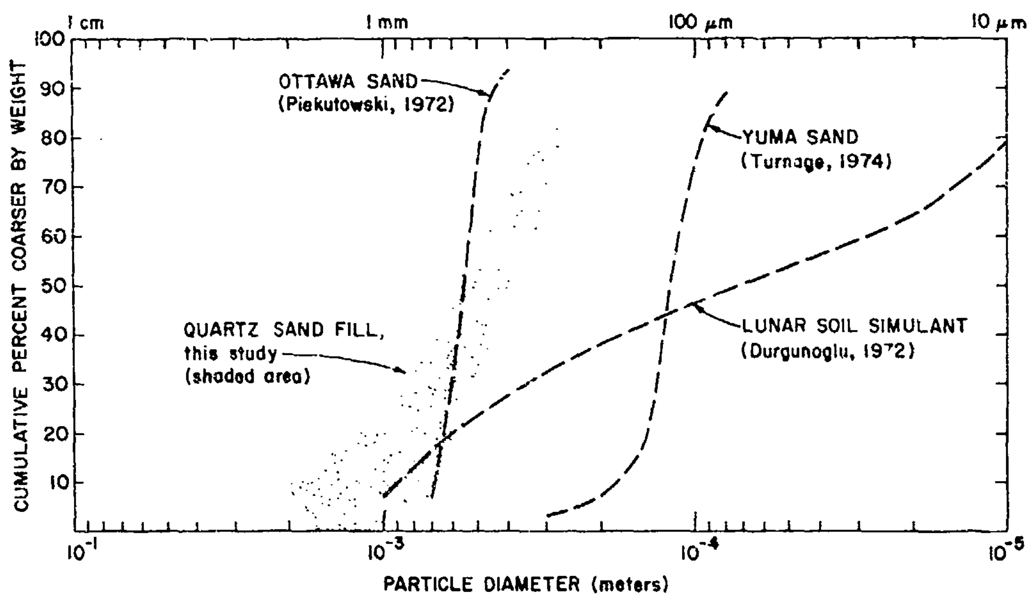

Figure 2. Particle Size Distribution of the Quartz Sand Fill at Ho l Range, Ft. Devens. Other sands and soil types are shown for comparison[22,23]

22. Durgunoglu, H.T. (1972) Static Penetration Resistance of Soils, PhD Thesis, University of California, Berkeley, California.

23. Turnage, G.W. (1974) Measuring Soil Properties in Vehicle Mobility Research; Resistance of Coarse Grained Soils to High Speed Penetration, Tech. Rpt No. 3-652, Report 6, U.S. Army Waterways Experiment Station, Mobility and Environmental Systems Lab., Vicksburg, Mississippi.

24. Fulmer, C.V. (1965) Cratering Characteristics of Wet and Dry Sand, The Boeing Company Report D2-90683-1, Seattle, Washington.

2.2 Materials

The pellets used in these experiments were spheres made of silica glass, acrylic resin, and aluminum alloy. The relative size and densities of the different pellet types are documented in Table 1.

Table 1. The Pellets Employed in These Experiments Were Made of Acrylic Resin, Glass, and Aluminum Alloy. The sizes and densities of the pellets are given in cm and grams/cm^3, respectively

Pellet Type		Diameter (cn.)	Density (gm/cm^3)
Acrylic Resin	red	1.97	1.02
	orange	1.24	1.19
Glass	yellow	1.53	2.20
	brown	1.43	2.70
	blue	1.55	1.92
Aluminum Alloy		1.27	2.84

The explosives used in these experiments were Hi-velocity gelatin, a mixture of 60 percent nitroglycerin and 40 percent inert material, and C-4, a mixture of 91 percent RDX (cyclonite) and 9 percent inert material. The relevant physical properties of these materials are compared with TNT and PETN (pentaeryghritol tetranitrate) in Table 2. The explosive charges were spherically shaped and centrally initiated by bridge wire electrical detonators. Two types of detonators were employed, an 'SSS' EB Cap, Strength No. 8, sold by Dupont and an M6 EB Cap, Strength No. 12, which is the Standard Army EB Cap.

2.3 Experimental Procedure

Pellets were emplaced within the test material 2 to 28 hours before the experiment (see Figure 3). Typically, several groups of pellets would be buried, with each group emplaced at a common depth along an imaginary horizontal line radial to a vertical centerline through the explosive charge. The radial range of an individual pellet was determined to within ± 0.125 in. (measured from surface ground zero); its depth of burial was determined to within ± 0.25 in. (measured from the original ground surface).

Table 2. The Physical Properties of the Hi-Velocity Gelatin and C4 Explosive Employed in This Study are Compared With Other Commonly Used Types of Explosives

	TNT (Trinitrotoluene)	Hi-velocity gelatin 60% nitroglycerin 40% inert	C4 9 % RDX 9% inert	PETN
Heat of Explosion (cal/g)	1080.	1204.	1120.	1385.
Density (g/cm^3)	1.6	1.3	1.6	1.7
Detonation Velocity (m/sec)	~6700	~6000.	~8050.	~8300.
Relative Quickness*	1.0	0.87	1.34	—
TNT Equivalent Weight	1.0	0.85**	1.30	—

*Relative 'quickness' is a military rating applied to different explosives on the basis of their explosive energy, density, and detonation velocity.

**TNT equivalent weight for Hi-velocity gelatin based upon relative 'quickness' and the results of the brisance sand test and ballistic pendulum test.

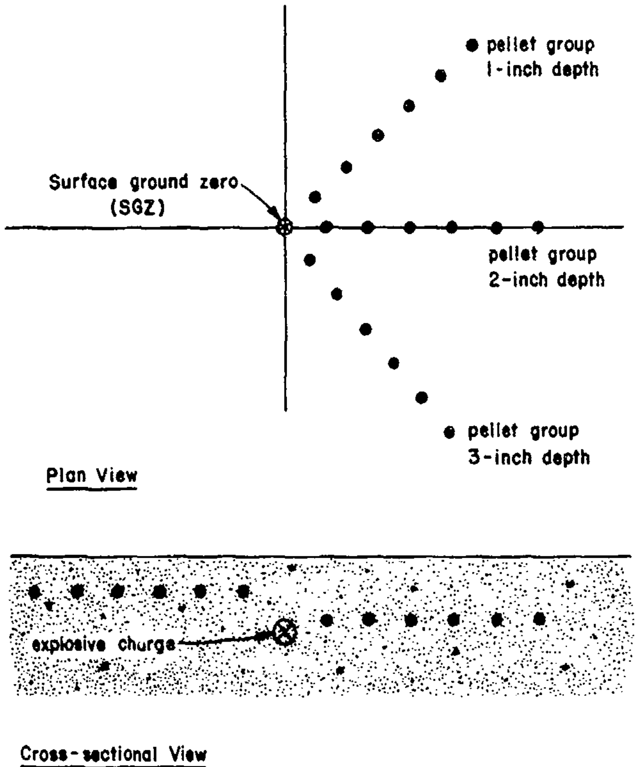

Figure 3. Schematic Map of Pellet Emplacement. A variety of pellet groups emplaced at different depths are excavated by the explosion. (Note pellet size is greatly exaggerated)

In-situ soil moisture was monitored by a Soiltest speedy moisture tester which measures the gas pressure generated by a mixture of calcium carbide reagent and test site material. The moisture content of the upper 0.3 m of the test site ranged from extremes of 1.5 wt percent to 9.0 wt percent but more typically equaled 1.5 to 5.0 wt percent.

Experiments were conducted on good weather days when local wind conditions were suitably calm. Even so, higher level gusts with velocities on the order of 1.0 m/sec may have influenced the trajectories of some pellets.

After a test shot, the pellets were relocated and their range from the center of the crater determined to within ± 0.125 in.

3. PELLET BEHAVIOR

In order to describe the translation of the bulk of the crater ejecta by tracking artificial pellets, the pellets should ideally behave as point masses during the cratering event. This means that the pellet could be replaced by a quartz particle and the quartz particle would be translated to the postshot range observed for the pellet. Clearly this is not the case. The pellet sizes are necessarily larger than the average or median size of quartz grains in order to permit postshot identification. Air drag resistance to pellet motion depends upon its velocity, surface area, and the appropriate drag coefficient. While the surface area of the pellets is larger than that of the quartz grains, the drag coefficient characterizing the larger pellet sizes should generally be less than the drag coefficient to the quartz grains.[25] These counterbalancing effects make it difficult to contrast pellet translation ranges with the throwout distances of quartz grains of comparable density initially accelerated to similar ejection velocities. However, the ballistic studies of Sherwood[25] indicate that pellet behavior should generally overestimate the translation of the smaller sized quartz sand.

The initial acceleration of material ejected by the explosive cratering event is produced by (1) the interaction of the individual particle with the compressional stress wave initially generated by the explosion and subsequent rarefaction waves reflected from the free surface of the ground, and (2) the interaction of the individual particle with the high velocity gases produced by the detonation of the explosive.

The effect of the size difference between the quartz grains and the artificial pellets on the relative particle accelerations imparted by the stress wave interaction mechanism is difficult to assess. In order to avoid differential accelerations of the in situ and emplaced materials, the strength of the pellet-quartz sand interface should approximate the strength of the quartz sand. It is not clear that this is the case. Recovered pellets occasionally have cone-shaped cappings of quartz sand that appear to have been compressed or molded onto the pellet surface. This may indicate that grain interaction initially accelerates some pellets to ejection velocities which exceed the velocities of quartz grains initially situated in similar preshot positions.

The velocity imparted to an individual particle by the accelerated gases vented from the expanding crater cavity will be proportional to the particle cross section. Therefore, the larger cross section of the pellets may cause them to be ejected at initial velocities greater than the velocity that would be imparted to a smaller quartz particle originally situated in a similar position. This would imply that the

---

25. Sherwood, A. E. (1967) Effect of air drag on particles ejected during explosive cratering, Jour. Geophys. Res. 72:1783-1791.

postshot pellet range represents a maximum estimate of the postshot range of a quartz particle originally in a similar position.

It is difficult to quantitatively estimate the extent to which these different effects influence pellet motion. In addition, variations in pellet translation can result from (1) azimuthal variability in the detonation wave that travels through the explosive, (2) the natural heterogeneity of the quartz sand test medium, and (3) the variability of local air currents. The densities of the pellets bracket the range of density of the natural materials that make up the quartz sand fill. Therefore, by considering both size and density, the actual behavior of an individual pellet during the cratering event may best represent the behavior of the coarsest fraction of the natural test material. In a later section, the translation histories of a group of pellets lying in a common radial direction will be compared with the translation of colored quartz sand tracer materials.

4. RESULTS

The pellet experimental program can be divided into three phases. The purpose of the first group of test shots was to determine the effects of charge size on the lateral translation of the artificial pellets. In this series of experiments, the explosive charge weight was varied from 1 to 4 lb at a constant scaled-depth-of-burst (SDOB). The second phase of experiments was designed to investigate the effect of variable scaled-depth-of-burst on the postshot pellet distribution. In this explosive series the charge weight was constant (5 lb) and the scaled-depth-of-burst varied from 0.20 approximately 0.55 ft/(lb TNT)$^{1/3}$. In the final phase, the generality of earlier results was tested by repeating the second phase of experiments using another type of explosive and different pellet materials. The results of the three phases will be discussed in this section. A compilation of the experimental field data is presented in Appendix A.

4.1 Crater Dimensions

The relationship between crater dimensions and the scaled-depth-of-burst of the explosive charge for all the craters produced by this experimental program is presented in Figure 4. For comparison, the crater depth (below rim crest)/radius (rim crest radius) ratios observed for a series of smaller scale experimental craters produced at the University of Dayton Research Institute (UDRI) are also shown in Figure 4C (see Piekutowski, 1974).[26]

26. Piekutowski, A. J. (1974) Laboratory Scale High Explosive Cratering and Ejecta Phenomenology Studies, University of Dayton Research Institute, AFWL-TR-72-155, Air Force Weapons Lab., Kirtland AFB, Albuquerque, New Mexico.

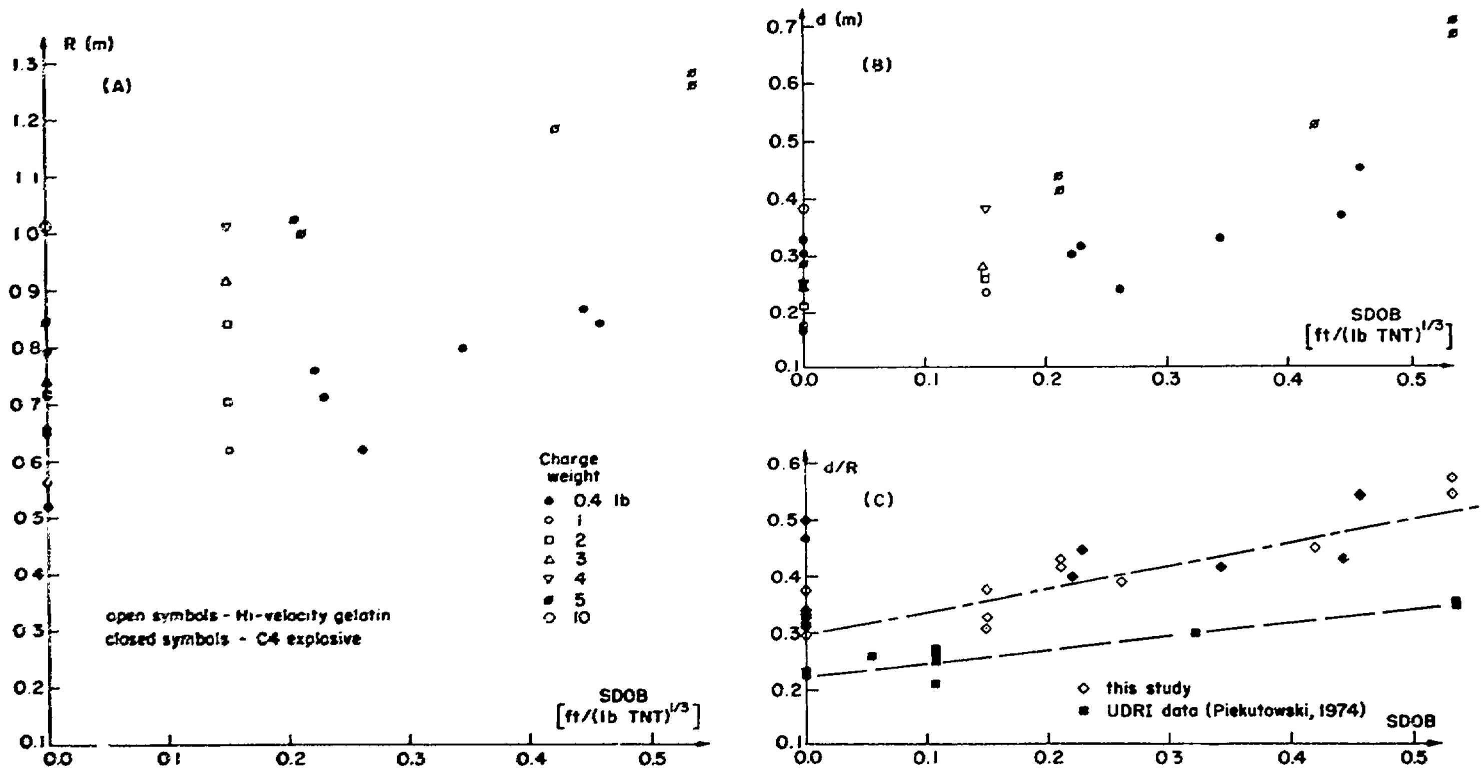

Figure 4. (A) Crater Rim Crest Radius R as a Function of Explosive Scaled Depth of Burst (SDOB). Open symbols represent Hi-velocity gelatin explosive; closed symbols represent C4 explosive. (B) Crater Depth d (measured from crater rim crest) as a function of explosive SCOB. (C) Ratio of crater depth (measured from crater rim crest)/rim crest radius as a function of explosive SDOB. In comparison, small explosion craters produced at UDRI are consistently shallower

The explosion craters produced by the present experimental series in quartz sand are consistently deeper and more bowl-shaped than the smaller scale UDRI craters. This probably reflects the greater natural cohesion of the quartz sand fill used in this study in contrast to the Ottawa sand employed in the UDRI experiments.

4.2 Presentation of Data

McGetchin et al[27] have suggested that the postshot range r of a mass point ejected by an explosive cratering event can be related to its preshot range x, measured from surface ground zero, by a simple power-law expression of the form

$$\frac{r}{R} \propto \left(\frac{x}{R}\right)^{c} , \qquad (1)$$

where R is the crater radius and the exponent c is a negative number. The form of Eq. (1) is particularly useful for comparing the results of a series of pellet experiments since the radial distances r and x have been normalized to the radius of the apparent crater lip, R. These normalized ranges permit comparison of the results of this study with explosive cratering events conducted at different scales.

A graphical representation of the experimental data is schematically outlined in Figure 5A. A linear plot of the power-law expression [Eq. (1)] for a variety of values of c produces a family of curves that converge as x/R approaches 1.0, or, in other words, near the crater rim where x = R. Larger negative values of c correspond to greater distances of radial translation for groups of pellets emplaced at a common depth. It is more convenient for the purpose of this study to consider the pellet data in the logarithmic coordinate system shown in Figure 5B.

A logarithmic plot of Eq. (1) yields a family of straight lines which similarly converge near the crater rim where $\log_{10}(x/R = 1.0) = 0$. Representation of the experimental pellet data in this form will reveal: (1) how accurately Eq. (1) describes the postshot distribution of pellets (note that a straight line fit to the experimental data would verify that the power-law expression provides a 'perfect' description of the relationship between preshot and postshot pellet position); (2) the approximate value of c for groups of pellets emplaced at specific depths within the test medium (note that the slope of a line, and not its absolute position within the logarithmic plot, defines the exponent); and, (3) the approximate radius of the true crater of excavation (note that the R measured experimentally is the rim crest radius). Material has not been excavated out to the rim crest radius R

27. McGetchin, T.R., Settle, M., and Head, J.W. (1973b) A model for the distribution of impact crater ejecta and its implications, EOS Transactions Am. Geophys. Union 54, No. 4:357.

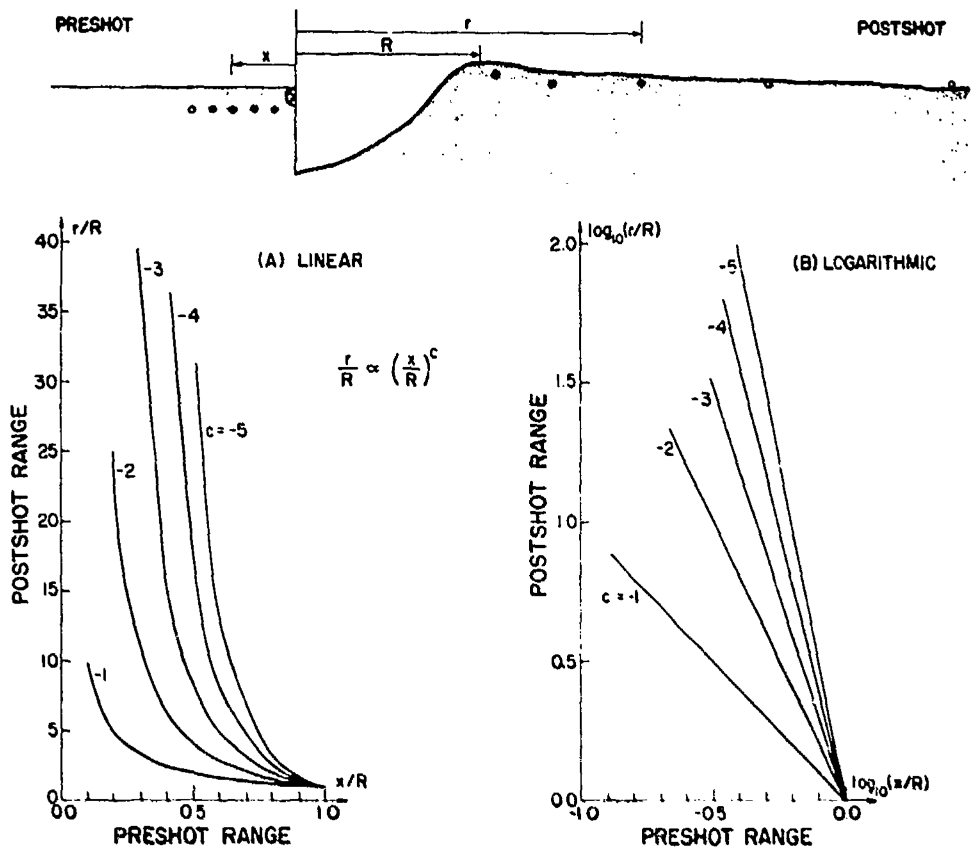

Figure 5. The Postshot Range r of a Mass Point Can Be Related to Its Preshot Range x (measured from surface ground zero) by a Power Law Expression. Figure 5A shows a linear plot of such an expression; 5B shows a logarithmic plot of the same expression. Data presented in this report will be plotted in the logarithmic format

since the material underlying the apparent rim crest consists of ejecta and structural uplift. The true limiting range at which material has been excavated can be approximately defined as the range x/R at which a straight line logarithmic fit to the pellet data equals 0.00. Graphically, this means that a straight line logarithmic fit to the actual pellet data will not pass through $\log_{10}(x/R = 1.0) = 0.00$; however, the range x/R at which it crosses the line $\log_{10}(r/R = 1.0) = 0.00$ will correspond approximately to the limiting range at which material was ejected by the cratering event (that is, the true radius of the crater of excavation).

Figure 5B also demonstrates the difficulty in determining an accurate value for the exponent c for a group of pellets that are transported to relatively small postshot ranges. This is the range of values of r/R in which the straight lines in Figure 5B converge. The recovery of pellets transported to large radial ranges (that is, the region in which the straight lines diverge in Figure 5B) is extremely valuable in distinguishing between different values of c.

4.3 Effect of Charge Size on Postshot Pellet Distribution

Figures 6 and 7 show the results of two series of explosive cratering experiments in which the size of an explosive charge of Hi-velocity gelatin was varied from 1 to 4 lb at a constant scaled-depth-of-burst of 0.00 and 0.15 ft/(lb TNT)$^{1/3}$, respectively. Both acrylic and glass pellets were simultaneously employed in these two series of explosion cratering experiments. The pellet data in Figures 6 and 7 demonstrate that the acrylic resin and the silica glass pellets were transported to generally similar normalized ranges by the individual cratering events. No consistent discrepancy exists between the postshot distributions of the two types of pellet materials.

A straight-line fit to the experimental pellet data appears to be a reasonable approximation of the lateral translation of individual pellet groups emplaced at different preshot depths. The reference line c = -4 offers an approximate description of the distribution of postshot ranges for the group of pellets nearest the original ground surface for both SDOB = 0.00 and SDOB = 0.15 ft/(lb TNT)$^{1/3}$.

In Figure 6 (SDOB = 0.00) the deeper pellet group, originally situated at a depth of 2 in., is translated to significantly shorter ranges than the pellet group initially situated at a 1-in. depth. This consistent relationship, successively deeper levels of material being transported to successively shorter postshot ranges, results in the inverted stratigraphy observed in the rim ejecta deposit produced by larger scale cratering in layered materials. However, in Figure 7 (SDOB = 0.15) the difference between the postshot positions of pellets, originally at a 1-in. and 2-in. depth within the quartz sand test medium, is much less. This is because both the 1-in. and 2-in. depths within the test medium will behave as near-surface 'layers' during the deeper SDOB = 0.15 event. Even in Figure 7, the deeper pellets generally travel to shorter postshot ranges and lie below the postshot range curves of pellet groups originally situated nearer the ground surface.

A further comparison of Figure 7 with Figure 6 suggests that the slope of a straight line fit through the 1-in. pellet data of Figure 7 (not shown) would generally be steeper than a similar straight line fit in Figure 6 (see data in Appendix A). In relation to the configuration of the explosive charge, the 1-in. pellet group in the SDOB = 0.15 case lies at a 'shallower' level than the 1-in. pellet group in the SDOB = 0.00 case and shallower levels <u>should</u> be translated farther. Steeper curves are indicative of greater lateral dispersion of ejected material and hence a more energetic excavation process at specific depths and explosive SDOB.

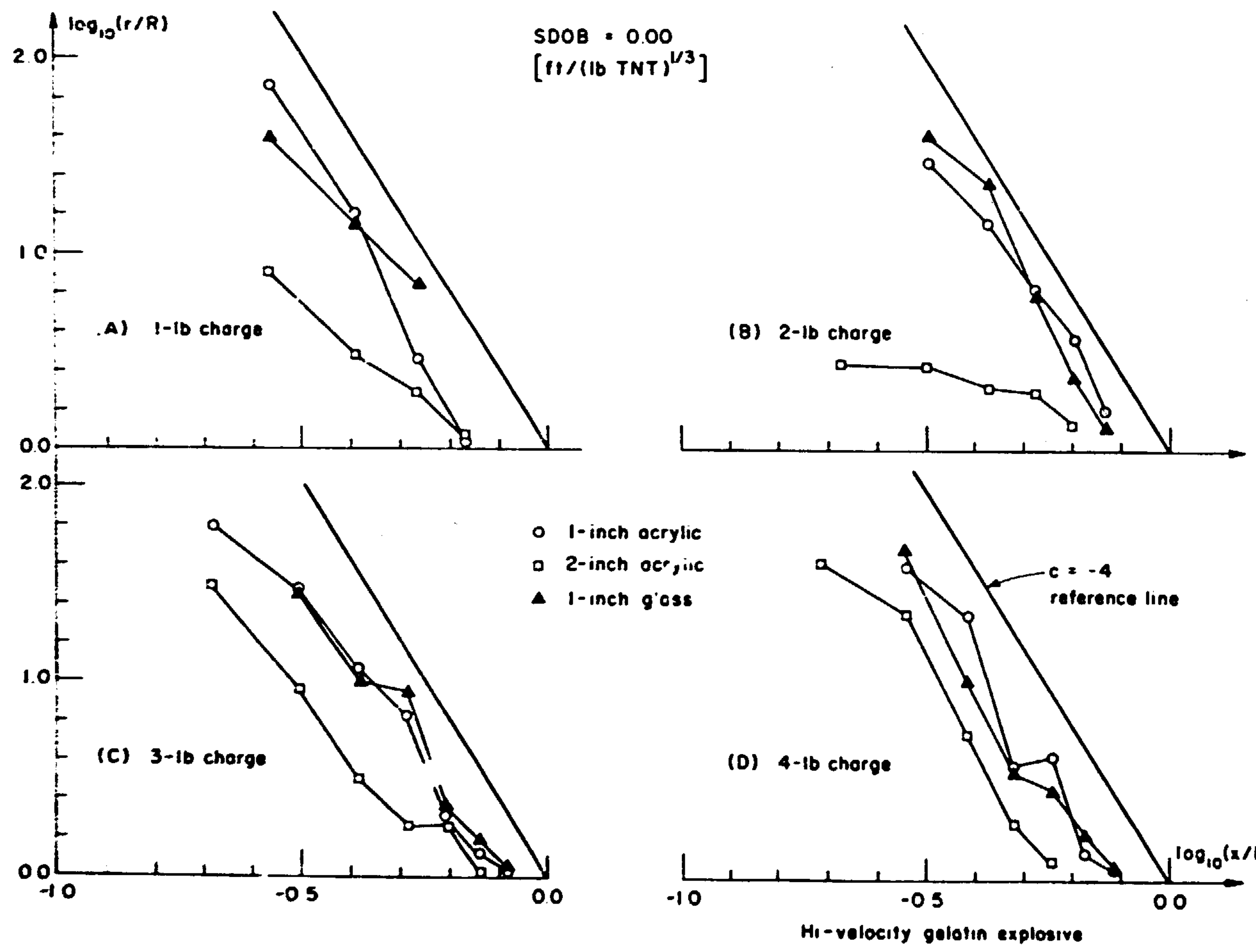

Figure 6. Distribution of Normalized Pellet Postshot Range for a Series of Experiments Employing Explosive Charges of Various Weights at a Constant SDOB = 0.00 ft/(lb TNT)$^{1/3}$. (A) 1-lb charge; (B) 2-lb charge; (C) 3-lb charge; (D) 4-lb charge. Hi-velocity gelatin was used in this experimental series. The label "1-in. acrylic" refers to a group of acrylic resin pellets emplaced at a 1-in. depth within the quartz sand prior to the explosion (see Table 1 for other pellet types)

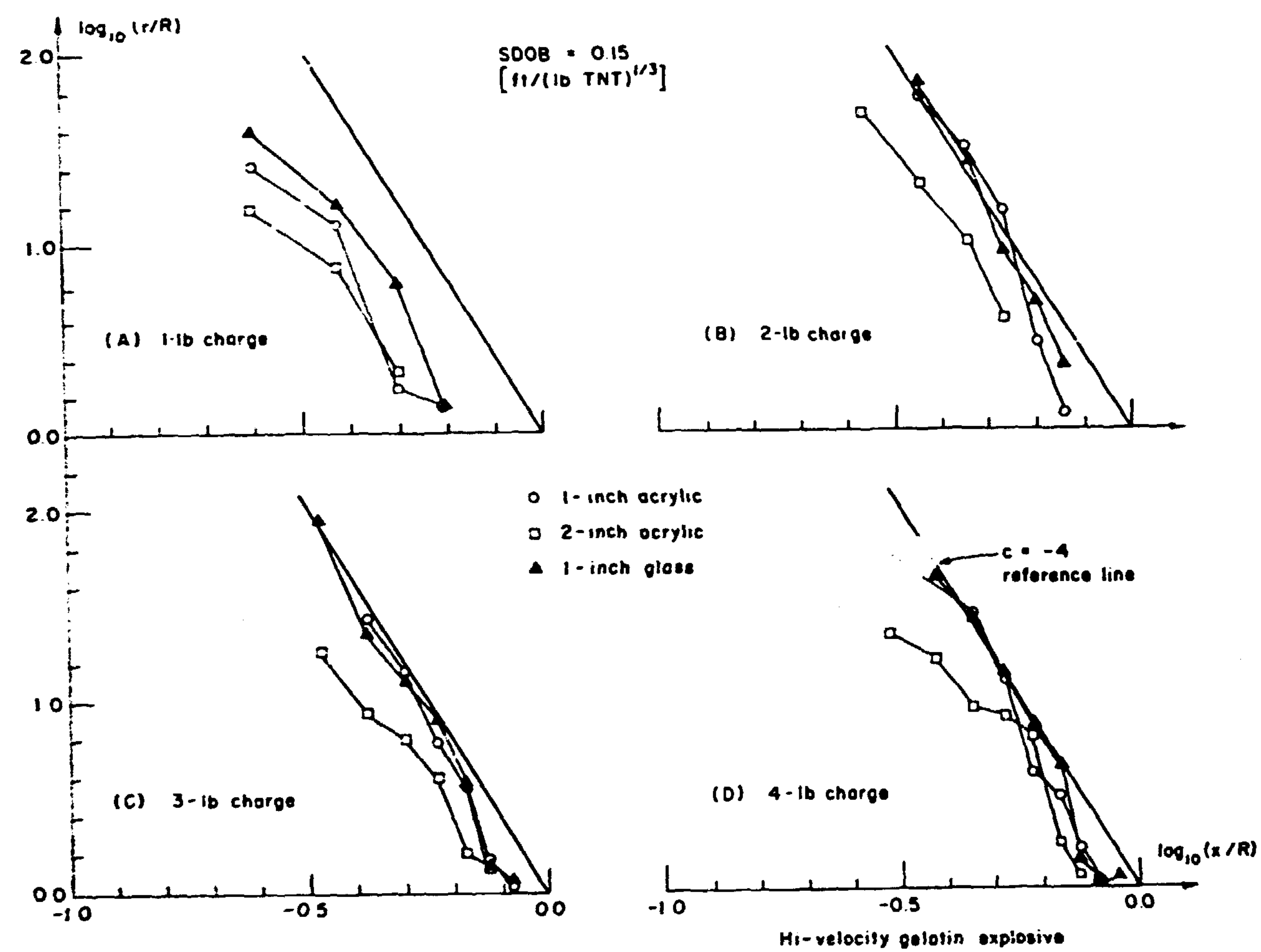

Figure 7. Distribution of Normalized Pellet Postshot Range for a Series of Experiments Employing Explosive Charges of Various Weights at a Constant SDOB = 0.15 ft/(lb TNT)$^{1/3}$. (A) 1-lb charge; (B) 2-lb charge; (C) 3-lb charge; (D) 4-lb charge. Hi-velocity gelatin was used in this experimental series. The label "1-in. acrylic" refers to a group of acrylic resin pellets emplaced at a 1-in. depth within the quartz sand prior to the explosion (see Table 1 for other pellet types)

This effect arises in the experimental data from a nonlinear increase in the coupling of explosive energy into the quartz sand test medium with increasing SDOB particularly in the near-surface range of SDOB from 0.00 to approximately 0.15 ft/(lb TNT)$^{1/3}$. In addition, the lateral confining pressure of the quartz sand increases with depth. This stress inhibits the growth of the crater and limits initial ejection angles to generally higher values (measured from the ground surface) with increasing SDOB. Higher ejection angles will tend to limit the lateral dispersion of crater ejecta. The pronounced steepening of the Figure 7 (SDOB = 0.15) curves can thus be interpreted in terms of an increase in the efficiency of explosive coupling, which is not cancelled by the corresponding increase in lateral confining pressures. At greater SDOB, the increase in confining pressure (which inhibits crater growth) compensates the increase in coupling efficiency (which promotes the formation of larger craters).

Figures 6 and 7 summarize the distribution of postshot pellet ranges for explosion experiments conducted at a constant SDOB, over a 1- to 4-lb range of charge size. Inspection of the pellet data from a particular preshot burial depth in each case demonstrates no consistent change in lateral translation of the pellet group with variation of the size of the explosive charge. Figure 7A (SDOB = 0.15, 1-lb charge) appears slightly anomalous in comparison with the other three experiments performed at SDOB = 0.15 ft/(lb TNT)$^{1/3}$. The cause of this discrepancy is unknown. However, the uniformity of the results of the three other experiments suggests that heterogeneity within the test site material and/or transient wind conditions may account for the pellet data presented in Figure 7A.

Finally, extrapolation of a straight line fit to the pellet data in both Figures 6 and 7 would intersect the abcissa $\log_{10}(r/R = 1.0) = 0$ at $\log_{10}(x/R) = -0.05$ to -0.15. This implies that the radius of the true crater of excavation is approximately equal to 70 to 90 percent of the measured rim crest radius.

4.4 Effect of Explosive Scaled Depth of Burst on Postshot Pellet Distribution

In order to observe the effect of the variable explosive SDOB on the translation of material ejected by an explosive cratering event, a series of experiments employing 5-lb Hi-velocity gelatin charges was conducted at SDOB ranging from 0.20 to 0.55 ft/(lb TNT)$^{1/3}$. The distribution of postshot pellet ranges for pellet groups emplaced at 2-in. and 3-in. depths in the quartz sand test medium are shown in Figure 8.

Surprisingly, the pellet data in Figures 8A (SDOB = 0.21) and 8B (SDOB = 0.42) reveal that the near-surface pellet groups (2 to 3 in.) within the quartz sand have been translated to normalized postshot ranges comparable to the normalized throwout distances observed for the corresponding near-surface pellet

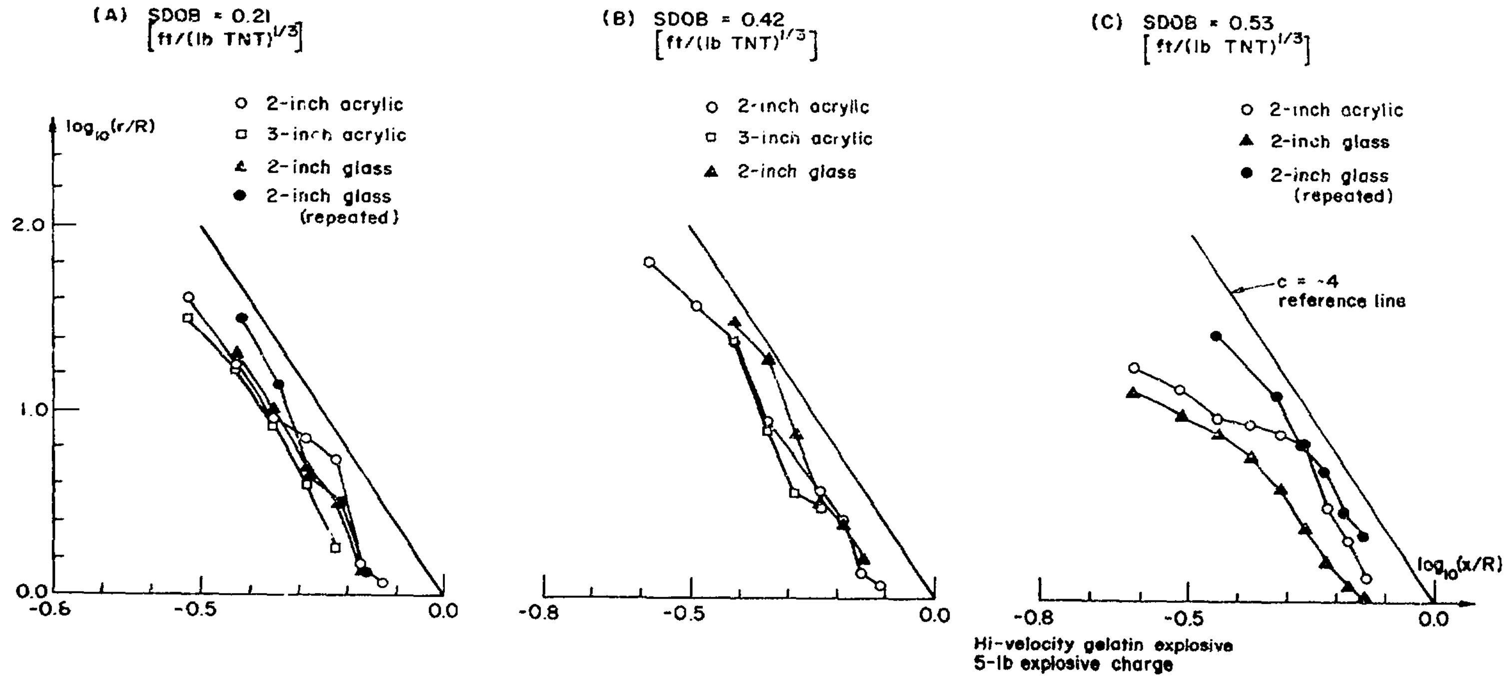

Figure 8. Distribution of Normalized Pellet Postshot Range for a Series of Experiments Employing Explosive Charges of Constant Size at a Variety of SDOB. (A) SDOB = 0.21 ft/(lb TNT)$^{1/3}$; (B) SDOB = 0.42 ft/(lb TNT)$^{1/3}$; (C) SDOB = 0.53 ft/(lb TNT)$^{1/3}$. Hi-velocity gelatin was used in this experimental series. The label "1-in. acrylic" refers to a group of acrylic resin pellets emplaced at a 1-in. depth within the quartz sand prior to the explosion (see Table 1 for other pellet types)

groups excavated by the surface burst test series (see Figure 6, SDOB = 0.00). In both cases, a least-squares fit of a straight line through the experimental pellet data would be reasonably approximated by Eq. (1) with the exponent c representing the slope of the line approximately equal to -4 ± 1 (see Appendix A).

The pellet data in Figure 8C (SDOB = 0.53) is somewhat ambiguous. The translation of the two groups of silica glass pellets emplaced at a 2-in. depth differs. The trend of the data from the repeated experiment is similar to the dominant trends in Figures 8A (SDOB = 0.21), 8B (SDOB = 0.42), and 6 (SDOB = 0.00). However, the slope of a straight-line fit to the 2-in. pellet data from the initial experiment at a SDOB = 0.53 ft/(lb TNT)$^{1/3}$ is shallower, suggesting a value of $c \cong -2$. The cause of this anomalous distribution of normalized pellet throwout ranges cannot be resolved. In the absence of any consistent trend in the data for the other buried cratering events [that is, Figures 8A (SDOB = 0.21) and 8B (SDOB = 0.42)], it is possible to attribute these relatively shallower sloping curves to heterogeneous physical properties within the test site material and/or transient wind conditions. Alternatively, this variation may be real in the sense that it indicates a decrease in the ability of the explosive cratering event to laterally transport ejected material at relatively larger SDOB. With increasing depth-of-burst of the explosive, the explosive energy released upon detonation becomes increasingly confined. Thus, since particle accelerations are initially directed radially away from the explosive, a transition may occur with increasing SDOB at which lateral particle motions are suitably confined to produce a decrease in postshot throwout ranges. For the particular charge size and quartz sand medium used in these experiments, the pellet data shown in Figure 8C (SDOB $\cong$ 0.53) may be indicating a transition in the ability of an explosive cratering event to laterally translate material at a SDOB $\cong$ 0.55 ft/(lb TNT)$^{1/3}$. This would suggest that within a certain range of SDOB bracketed by $0.00 < \text{SDOB} < 0.55$ ft/(lb TNT)$^{1/3}$, the excavation process achieves a maximum ability to laterally translate ejected material beyond the crater rim. The discrepancy between the pellet data for the 2-in. level at a SDOB = 0.53 ft/(lb TNT)$^{1/3}$ (Figure 8C) may reflect the effect of variable physical properties of the test material on the actual value of such a transitional SDOB.

Comparison of Figure 8 with Figure 7 (SDOB = 0.15) demonstrates that the steepest pellet-data curves (implying the greatest lateral translation distances) observed in all test series are associated with the SDOB = 0.15 ft/(lb TNT)$^{1/3}$ explosive cratering events. This relationship is consistently observed in Figures 7B, 7C, and 7D. Therefore, the distributions of postshot pellet ranges shown in Figure 7 (SDOB = 0.15) cannot reflect natural variations in the quartz sand or transient wind conditions. This observation supports the concept of a critical SDOB at which the lateral translation of ejected material is at a maximum. Furthermore, it suggests that this critical SDOB is in the range 0.10 to 0.20 ft/(lb TNT)$^{1/3}$ for the quartz sand and 1- to 5-lb explosive charges employed in this study.

4.5 Effect of Experimental Materials on Postshot Pellet Distribution

A final series of explosive cratering experiments was conducted employing 1.0- and 1.1-lb charges of C4 explosive and spherical pellets made of aluminum alloy. A calibration test shot using acrylic resin, silica glass, and aluminum pellets and a Hi-velocity gelatin explosive was conducted at a SDOB = 0.26 ft/(lb TNT)$^{1/3}$ to compare the behavior of the three pellet types in a 'standard' explosive cratering event. The resulting postshot pellet distributions presented in Figure 9 show that the three pellet types are transported to generally similar normalized ranges.

The experimental test series employing the C4 explosive was conducted over a range of SDOB varying from 0.00 to 0.45 ft/(lb TNT)$^{1/3}$. The results presented in Figure 10 support the generality of Eq. (1) with $c \cong -4 \pm 1$ as an empirical description of the translation of near surface material ejected by an explosive cratering event at SDOB = 0.00 and at 0.23 < SDOB < 0.45. Unfortunately, no experiment was performed at a SDOB = 0.15 ± 0.05 ft/(lb TNT)$^{1/3}$ in the range of the critical SDOB suggested by the results of the earlier experimental series.

Figure 10 also demonstrates that deeper levels within the quartz sand test medium are translated to significantly shorter ranges at all SDOB. In Figure 10D (SDOB = 0.45), the results of two explosive cratering experiments conducted at the same SDOB are presented together. These results show in part the variability of the behavior of the quartz sand test medium which is ejected and transported by the cratering event. (Compare, for example, the data for the 3-in. pellet depth from the two experiments.) Figure 10D also shows that the lateral translation of successive depths within the crater of excavation can be described by a series of equations having the form of Eq. (1) with the exponent c varying from ~ -4 to ~ -1 with increasing excavation depth. The possibility of comprehensively describing the translation of material transported by an explosive cratering event will be explored in the following section.

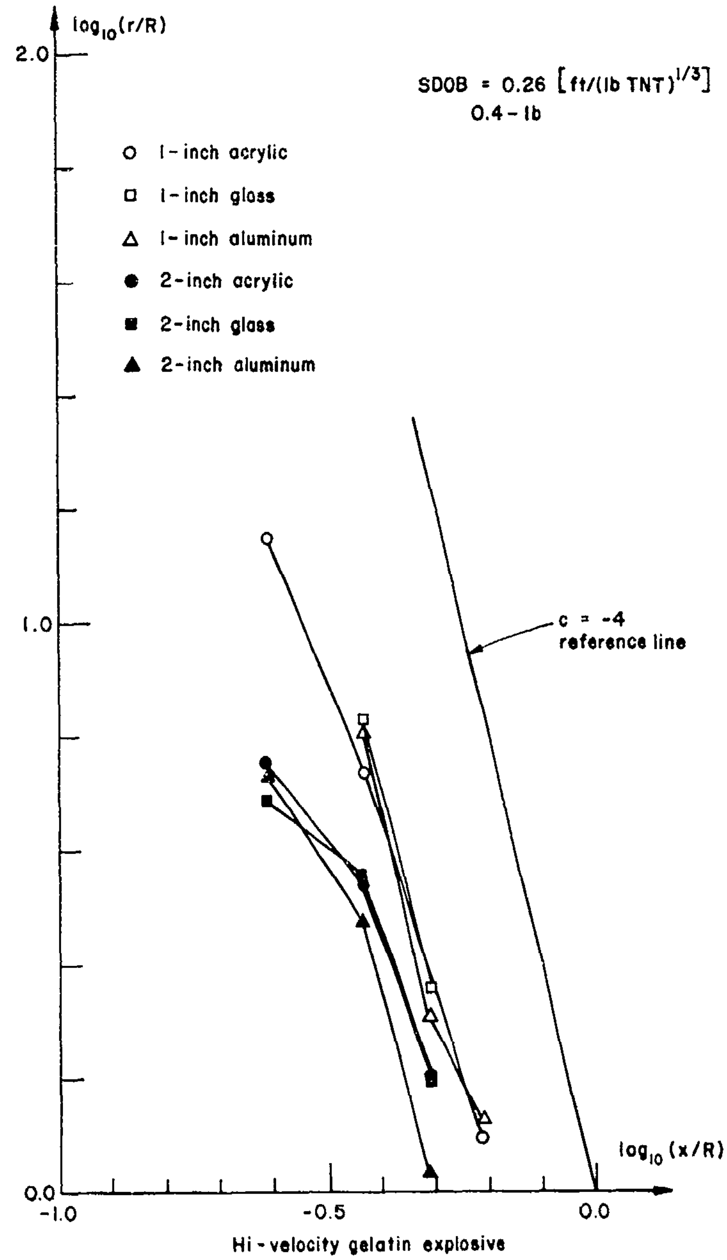

Figure 9. Distribution of Normalized Pellet Postshot Range for a Series of Experiments Employing a Variety of Pellet Materials and a 0.4-lb Charge of Hi-velocity Gelatin Explosive in a SDOB = 0.26 ft/(lb TNT)$^{1/3}$ Configuration. The label "1-in. acrylic" refers to a group of acrylic resin pellets emplaced at a 1-in. depth within the quartz sand prior to the explosion (see Table 1 for other pellet types)

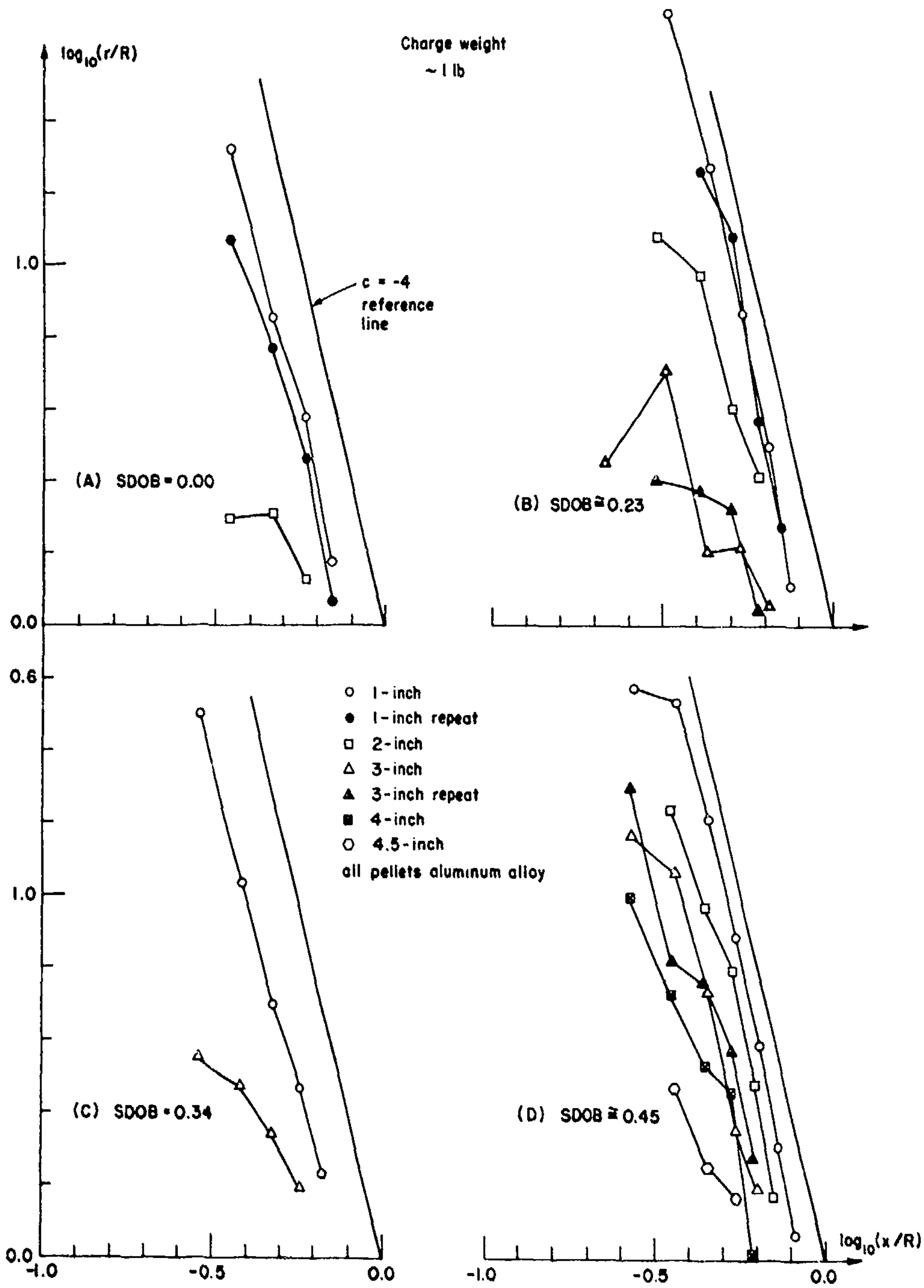

Figure 10. Distribution of Normalized Pellet Postshot Range for a Series of Experiments Employing Explosive Charges of Constant Size at a Variety of SDOB. (A) SDOB = 0.00 ft/(lb TNT)$^{1/3}$; (B) SDOB = 0.23 ft/(lb TNT)$^{1/3}$; (C) SDOB = 0.34 ft/(lb TNT)$^{1/3}$; (D) SDOB = 0.45 ft/(lb TNT)$^{1/3}$. C4 explosive was used in this experimental series. The label "1=in. acrylic" refers to a group of acrylic resin pellets emplaced at a 1-in. depth within the quartz sand prior to the explosion (see Table 1 for other pellet types)

5. DISCUSSION

The excavation process which accelerates material above the original ground surface is made up of two component mechanisms.[28,29] One mechanism is the complex interaction of the initial shock stress wave with the subsequent suite of rarefaction waves produced by reflection of the stress wave from the ground (free) surface. This family of rarefaction waves is essentially a broad relaxation pulse which provides for the continuous decompression of the shock-stressed material. The initial stress wave accelerates material radially away from the point of detonation while the rarefaction wave tends to re-orient the direction of individual particle velocity (see Gault et al[8]). Near the free (ground) surface the particle acceleration supplied by the stress and rarefaction waves act in a similar, outward direction. Material near the free surface is ejected at approximately twice the particle velocity to which material was initially accelerated by the stress wave. This phenomenon of stress wave interaction in the vicinity of the free surface has been termed 'spalling'. In hard rock materials, spalling creates new free surfaces below the original ground surface permitting continued stress wave-free surface interaction beneath the original ground surface.[30] In granular and soft rock materials, particle accelerations induced by the initial stress wave and the subsequent rarefaction waves do not act in the same direction below the immediate ground surface. The tensile rarefaction waves cause the radial flow field established by the initial stress wave to diverge. As a result, the acceleration of individual particles is re-oriented upward, contributing to the ejection of material beyond the transient rim of the growing crater and the plastic deformation of substrate material. This wave interaction phenomenon has been termed 'lateral flow' by Gault et al.[8] In both cases, spall and lateral flow, the kinetic energy of the ejected material is derived from the interaction of compressive and tensile stress waves propagating through the target or test material.

The second mechanism that excavates and ejects material from an explosion crater is gas acceleration. Nordyke[28] has described how the initial acceleration of ejected material can be significantly increased by the venting or expansion of gases produced by the detonation of the explosive materials.

Nordyke[28] has hypothesized that the wave interaction mechanism dominates the excavation process at shallow explosive depths-of-burst and is replaced by

---

28. Nordyke, M. D. (1961) Nuclear craters and preliminary theory of the mechanics of explosive crater formation, Jour. Geophys. Res. 66:3439-3459.

29. Short, N. M. (1965) A comparison of features characteristic of nuclear explosion craters and astroblemes, Annals N. Y. Acad. Sci. 123:573-616.

30. Horz, F. (1969) Structural and mineralogical evaluation of an experimentally produced crater in granite, Contributions Mineralogy Petrology 21:365-377.

the gas acceleration mechanism at larger depths-of-burst (see Figure 11). At intermediate depths-of-burst, both mechanisms are important. In turn, experimental investigations have attempted to relate the morphology and distribution of explosion crater ejecta deposits to the two components of the excavation process. For example, the study of pellet data from the Air Vent/Flat Top Series of

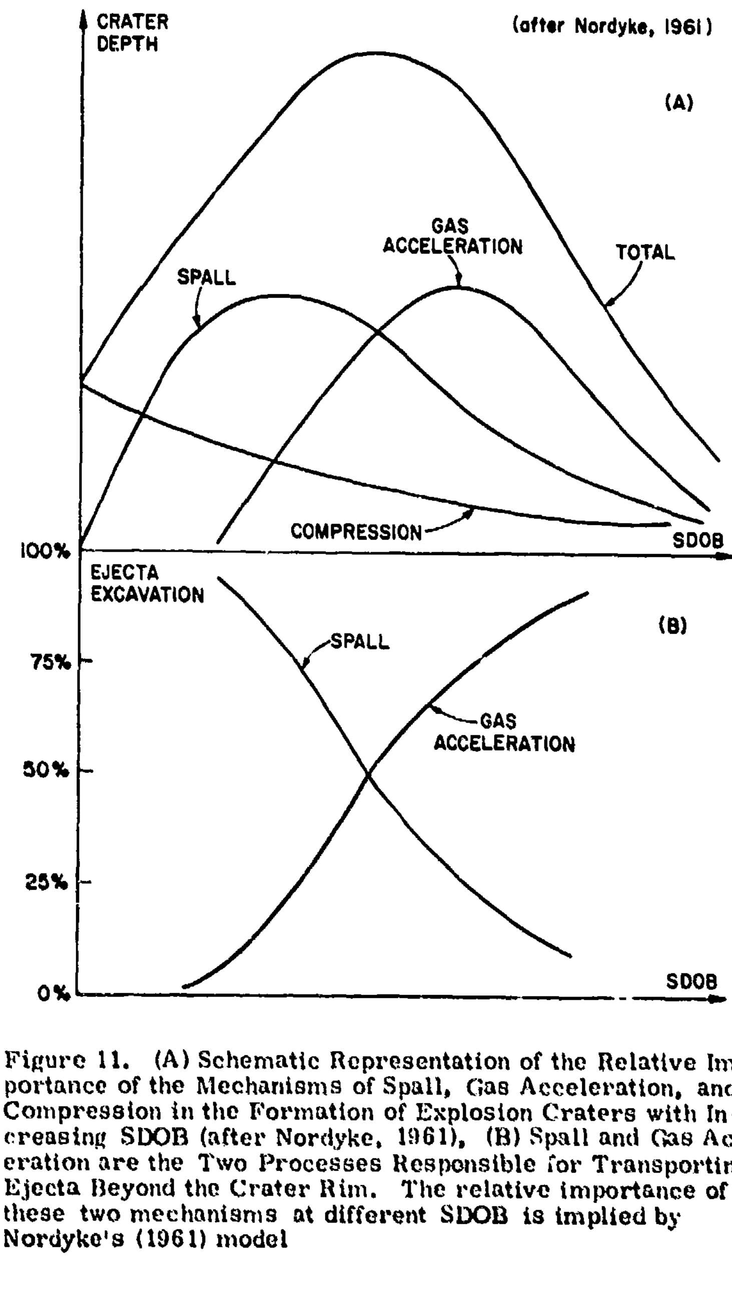

Figure 11. (A) Schematic Representation of the Relative Importance of the Mechanisms of Spall, Gas Acceleration, and Compression in the Formation of Explosion Craters with Increasing SDOB (after Nordyke, 1961), (B) Spall and Gas Acceleration are the Two Processes Responsible for Transporting Ejecta Beyond the Crater Rim. The relative importance of these two mechanisms at different SDOB is implied by Nordyke's (1961) model

explosion cratering experiments in playa and limestone mediums, led Ahlers[31] and Anthony[32] to characterize regions within the crater of excavation as sources of "ballistic ejecta" and "scoured ejecta" (Figure 12). These terms attempted to distinguish material that was accelerated and ejected into clearly definable ballistic trajectories (that is, "ballistic ejecta") from other material that appeared to be pushed or shoved up and over the crater lip (that is, "scoured ejecta"). Ballistic ejecta originated from near ground zero and regions adjacent to the explosive charge and was transported to large postshot ranges. Scoured ejecta originated from regions beneath and beyond the ballistic zone and it was transported to relatively small radial ranges (see also Merritt, 1968).[33]

The maximum acceleration due to spalling can be anticipated at surface ground zero where the magnitude of the stress wave at the time of reflection will be greatest (that is, the travel time of the shock wave at the time of reflection will be a minimum directly above the detonation point). The fact that the area adjacent to surface ground zero is the source region of ballistic ejecta suggests an association between this material and the spall mechanism. The additional observation that the ballistic ejecta travels to distant ranges and is thus initially accelerated to higher ejection velocities than scoured ejecta, also supports such an association. Alternatively, the source region of scoured ejecta is situated at some distance from the detonation point. The acceleration mechanism responsible for the acceleration of the scoured ejecta can be inferred to be somewhat weaker than the dominant ballistic ejecta mechanism since this material is translated to significantly shorter ranges. In this case, an association is implied between the scoured ejecta and the gas acceleration mechanism. However, neither of these mechanisms is solely responsible for the translation of individual ejecta particles. Both spall and gas acceleration contribute to the kinetic energy of an ejecta particle, though the combination of the two component accelerations is undoubtedly more complicated than the simple vector addition of these two forces for individual particles.

The results of Ahlers[31] and Anthony[32] indicate that each of the two different mechanisms may dominate the excavation process for significantly different

---

31. Ahlers, F. B. (1965) Crater Ejecta Studies - Flat Tops II and III, Project 1.5a, Ferris Wheel Series, Flat Top Event, POR - 3006, IIT Research Institute, Chicago, Illinois.

32. Anthony, M. V. (1965) Ejecta Distribution from the Flat Top I Event, Project 1.5b, Ferris Wheel Series, Flat Top Event, POR - 3007, The Boeing Company, Seattle, Washington.

33. Merritt, M. L. (1968) Ferris Wheel Series, Air Vent/Flat Top Events, Project Officers Report, Scientific Directors Summary, POR - 3000, Sandia Corporation, Albuquerque, New Mexico.

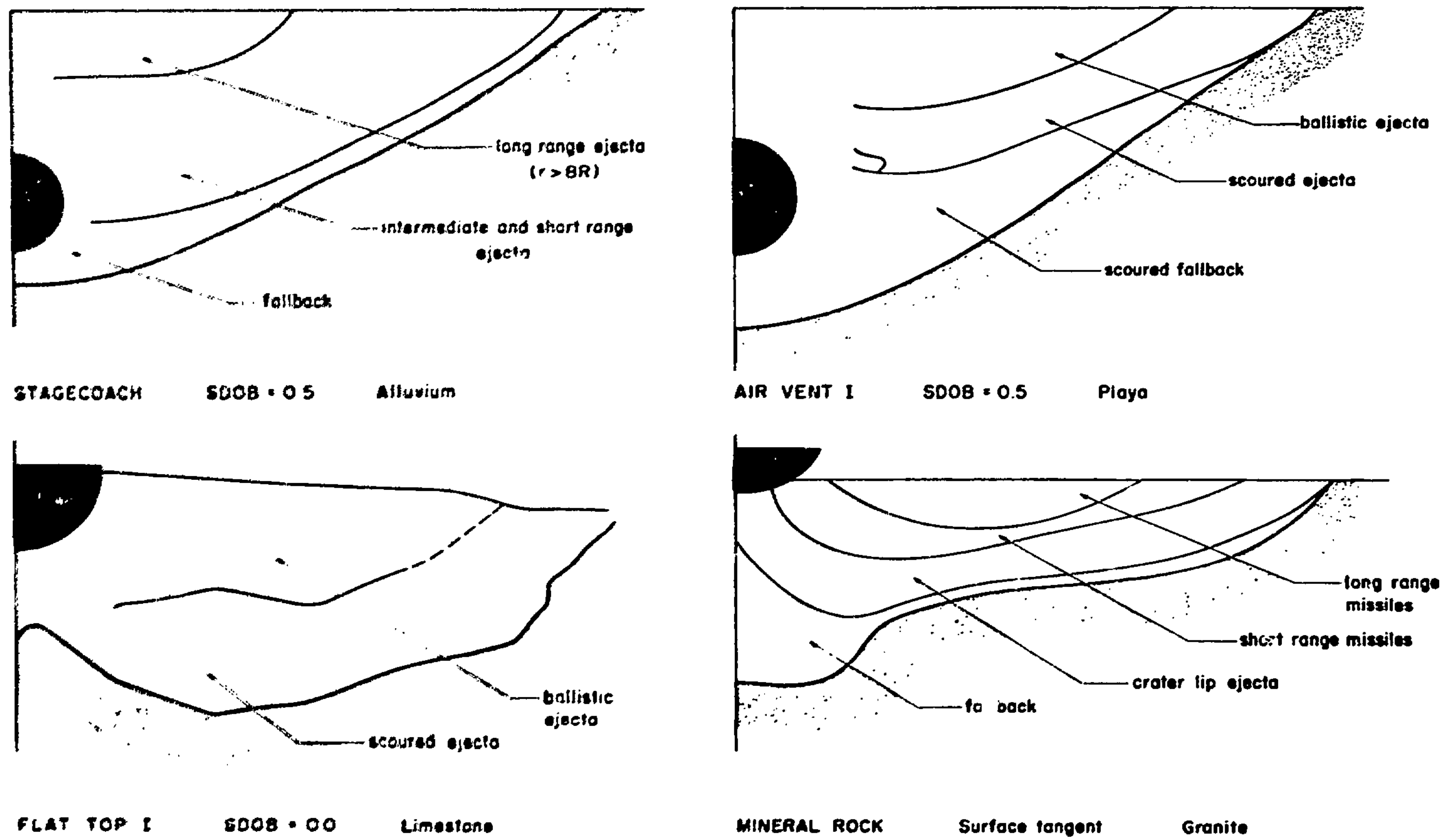

Figure 12. Ejecta Source Regions Within the Original Ground Surface for Large Scale Explosion Cratering Experiments (see text for references). Note that compression of substrate material, fallback, and post-excavation slumping may significantly restructure the geometry of the ejecta source region to produce the apparent crater. (SDOB is given in ft/(lb TNT)$^{1/3}$)

portions of the crater of excavation (see Figure 12). This is in addition to Nordyke's[28] hypothesis that each of the two different excavation mechanisms should dominate the overall excavation process at different depths-of-burst (see Figure 11). Furthermore, the relative position of the ballistic and scoured zones within the crater of excavation mapped by the pallet data from the Flat Top Series suggests that ballistic ejecta is unloaded at an earlier stage of crater formation and is chronologically followed by excavation of scoured ejecta (Figure 12).

The later studies of Henny and Carlson[1] were directed towards a quantitative description of the block distribution produced by explosive cratering in a hardrock basaltic medium. Their results characterize three modes of ejecta deposition:

> Mode I consists of a blanket of missiles extending from the continuous ejecta distribution being roughly symmetrical to the crater. Mode II consists of missiles forming tongue-like structural lineaments extending radially out from the crater. Mode III consists of a number of missile clusters and/or individual missiles superimposed upon the first two modes and extending from the immediate vicinity of the crater outward to the maximum depositional range.

These three depositional modes were then related to initial ejection conditions which determine the ballistic trajectories of individual particles. Mode I is interpreted as an extension of the continuous deposit ejected from the crater of excavation at relatively small angles (for example, less than 25° measured from the original ground surface). Mode II is interpreted as material initially ejected at intermediate angles (for example, 25° to 65°). Finally, Mode III material is inferred to be high-angle ejecta which remains in flight for longer periods of time and is generally superimposed upon the first two morphologies. Though the separate modes are interpreted as beginning and ending in order, all three may occur simultaneously at intermediate ranges.[1]

There is no straightforward relationship that defines the relative ejection velocity of particles which are ejected at different angles. Qualitatively, however, photographic investigation of the early stages of excavation suggests that ejection angle generally decreases as the radius of the transient crater increases.[17] Since material directly overlying the detonation point achieves the maximum ejection velocity, it is probable that the fastest material is ejected at the higher ejection angles (measured from the ground surface). Therefore, it is possible that the successively higher modes of ejecta deposit morphology are associated with both larger ejection angles and greater particle ejection velocities.[1]

The empirical description of the translation of pellet strings developed in the previous section [see Eq.(1)] is not related to specific excavation mechanisms. Rather, it expresses the observed relationship between pre-event and post-event pellet position without reference to the mechanics of excavation process. As suggested previously, it may be possible to extend the simple power-law expression to a description of the translation behavior of pellets emplaced at a variety of levels within the crater of excavation. Ideally, parametrization of the power-law exponent c in terms of relative depth within the crater of excavation and the scaled depth of burst of the explosive charge would permit a continuous description of pellet translation for a variety of explosive cratering events. This is attempted in Figure 13 where the value of the exponent c (that is, the slope of the straight line determined by a least-squares fit of the pellet translation data presented in Appendix A) is plotted as a function of relative depth within the crater (that is, the ratio of the depth of burial of individual pellet groups/depth of the fresh crater measured from the original ground surface) for a variety of SDOB. It appears that the variation in c can be generally described by an S-shaped curve trending from large negative values of c for shallow levels within the crater of excavation to smaller, limiting negative values of c for deeper levels. This conforms to the earlier qualitative observation that successively deeper levels within the crater of excavation are laterally translated to relatively shorter ranges since larger negative c values characterize larger radial translations. In the deeper portions of the crater of excavation, compressive deformation and plastic flow of the underlying material plays a significant role in crater formation. The methods of surveying preshot- and postshot-pellet positions employed in these experiments were not sufficiently accurate to warrant pellet emplacement at depths greater than approximately half the anticipated crater depths where the phenomenon of plastic flow would considerably complicate pellet translation.

Figure 13 describes the average behavior of the artificial pellets and the granular quartz sand test medium over the range of ground moisture conditions and localized particle size distributions, and the performance of the explosive charges over their effective energy yields and their effective yield of gaseous products which characterized the entire test program. However, the relative scatter over a range of depth and SDOB demonstrates that for a particular explosive cratering event (that is, SDOB = constant), the translation of pellets at different levels within the granular quartz sand is most variable near the surface and becomes less variable with increasing depth. In addition, the relative position of the approximate bounds which have been placed on the pellet data at different SDOB (Figures 13A, B, and C) indicate that within increasing SDOB the radial translation of near-surface pellet strings ($d < 0.2\,d_{cr}$) is significantly attenuated while the relative translation of intermediate levels within the crater of excavation ($0.2\,d_{cr} < d < 0.4\,d_{cr}$) remains approximately the same.

The possibility of a critical near-surface SDOB, at which pellet-translation distances achieve a maximum, is suggested by the large negative values of c associated with shallow depths ($d \sim 0.1\,d_{cr}$) for SDOB = 0.15 ft/(lb TNT)$^{1/3}$ in

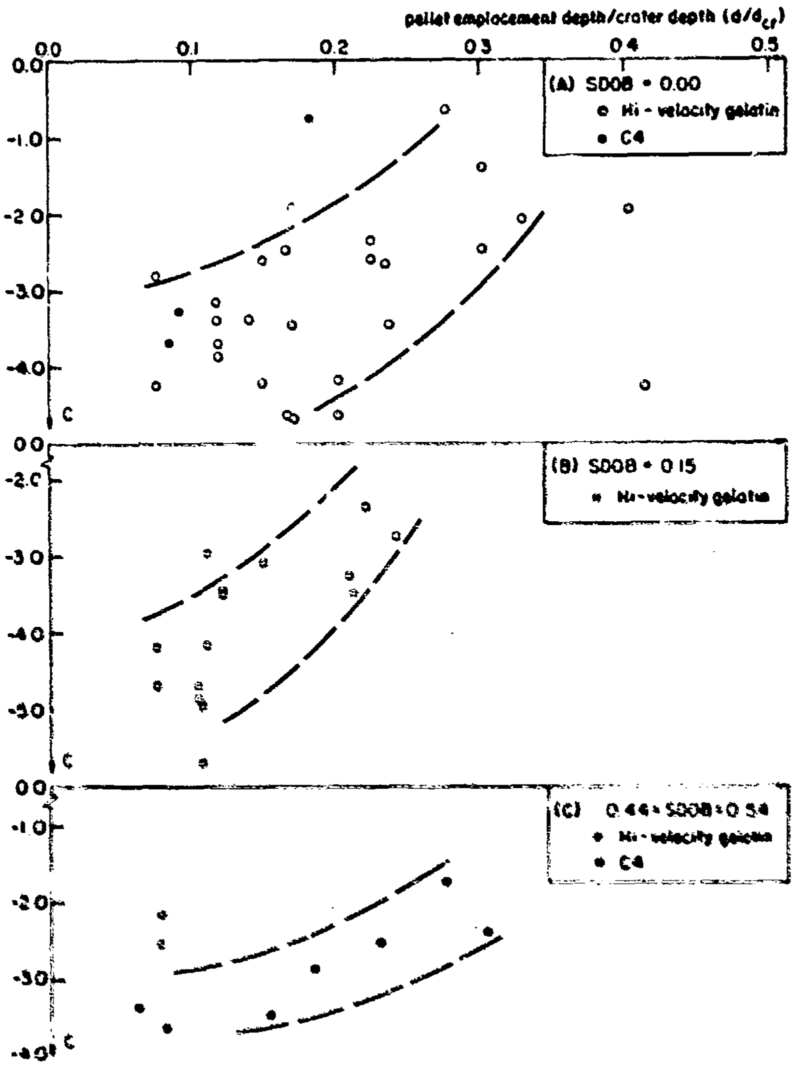

Figure 13. A Comparison of the Variation of the Exponent c (from Eq. 1) with Depth Within the Ejecta Source Region for a Variety of SDOB. This exponent describes the relative translation of the artificial pellets. (A) SDOB = 0.00 ft/(lb TNT)$^{1/3}$; (B) SDOB = 0.15 ft/(lb TNT)$^{1/3}$; (C) 0.44 $\leq$ SDOB < 0.54 ft/(lb TNT)$^{1/3}$. Note that the crater depth employed here is measured from the original ground surface

Figure 13B. Such a maximum has also been suggested by the preliminary results of the current U.S. Army program concerned with the effects of subsurface explosions, Project ESSEX.[34] In the context of the earlier discussion of excavation mechanisms, this value of SDOB may approximately mark the maximum in the lateral translation of ejected material produced by the combined effects of spall and gas acceleration shown schematically in Figure 11.

The results of this small-scale experimental program can be compared with two large-scale, 20-ton TNT explosive cratering events, in which detailed pellet experiments were also conducted. The results of these large-scale experiments, in which several hundred artificial pellets were used, are presented schematically as regions within the crater of excavation which are transported to some limiting postshot range. Such regions are delineated by equal postshot range contours within the crater of excavation similar to the generalized contours shown in Figure 12. The radial variation of the position of inferred isorange contours within the crater of excavation of the Stagecoach (SDOB = 0.50 ft/(lb TNT)$^{1/3}$, in alluvium) and Air Vent I (SDOB = 0.50 ft/(lb TNT)$^{1/3}$, in playa) events have been fitted to the power-law expression used in this study at different depths within the crater of excavation (see Vortman and MacDougall (1962) and Merritt (1968), respectively).[33,35] (Note that translation data was not available for material initially situated at ranges less than 0.2 crater radii from surface ground zero, see Figure 12.) The trend of the Stagecoach and Air Vent I curves in Figure 14 generally corresponds to the SDOB = 0.50 ft/(lb TNT)$^{1/3}$ data produced by the present study, but consistently lies at smaller negative e values. Such values indicate smaller normalized translation ranges for the emplaced pellets and are to be expected for larger scale events in which (1) test medium materials are better consolidated and (2) greater charge yields for events with similar SDOB require larger actual depths-of-burst which result in larger lateral confining pressures in the region of charge detonation (see Sun, 1970; White, 1973).[36,37]

The pellet-translation experiments presented in this study have employed loose, relatively dry quartz sand under very low confining pressures as a test medium.

---

34. Dishon, J. C. (1975) ESSEX - Diamond Ore Research Program: Ejecta Measurements Report - ESSEX I, Phase I, WES MP-E-75-3, U.S. Army Waterways Experiment Station, Explosive Excavation Research Lab., Livermore, California.

35. Vortman, L.J., and MacDougall, H.R., eds. (1962) Project Stagecoach: 20 Ton HE Cratering Experiments in Desert Alluvium, Final Report, SC-4596, TID-4500, Sandia Corporation, Albuquerque, New Mexico.

36. Sun, J.M. (1970) Energy counter-pressure scaling equations of linear crater dimensions, Jour. Geophys. Res. 75:2003-2027.

37. White, J.W. (1973) An empirically derived cratering formula, Jour. Geophys. Res. 78:8623-8633.

Thus, the values of c describing pellet-postshot distribution reported here should represent maximum negative values when compared with larger scale explosion events in other geological environments.

The results of the present study can also be compared with smaller scale explosion cratering experiments conducted at the University of Dayton Research Institute (UDRI) using ~ 2-gm lead azide charges in Ottawa sand.[26] Dyed sand was employed as a tracer material in a series of experiments in order to delineate translation ranges of material ejected from the crater of excavation.[38] Least-square fits to the power-law expression used in this study were performed using the data of Andrews[38] for SDOB = 0.00 and SDOB ≅ 0.11 ft/(lb TNT)$^{1/3}$, and are presented in Figure 14. (Note that translation data for material initially situated at ranges less than 0.2-crater radii was not well resolved and was not used in calculating the power-law exponents shown in Figure 14.) Remarkably, there is a similarity between the variation of the mapping exponent c, with depth within the crater of excavation for the small scale UDRI experiments and the much larger scale 20-ton experiments. In comparison, the normalized translation ranges of the artificial pellets employed by the present study are much greater than the normalized ejecta-translation ranges reported by the smaller scale experiments and the normalized pellet-translation ranges reported by the large-scale experiments. This contrast is particularly surprising with regard to the smaller scale (UDRI) experiments in which smaller lateral confining pressures would *a priori* have suggested greater normalized ejecta-translation ranges (that is, larger negative values of the exponent c) than the pellet-translation results of the present study.

The fact that the artificial pellets employed in this study are thrown to such anomalously large normalized ranges, indicates that they are not being translated in the same manner as the bulk of the ejecta. The critical difference between the experiments conducted here and the explosion events conducted at larger and smaller scales, is the relation of pellet size to ejecta-particle size. In the small-scale experiments, dyed sand was employed as the tracer material, and so the size of the "pellet" tracer was approximately equal to that of the ejecta particle. In the larger scale experiments, artificial pellets ranged in size from 3/8 to 1-1/2 in.,[33,35] while ejecta particles spanned a larger size range which included the sizes of the emplaced pellets. In this study, the artificial pellets were consistently larger than the coarsest fraction of the quartz sand fill. Therefore, the similarity of ejecta-translation results of the small-scale UDRI experiments (pellet (dyed sand)

38. Andrews, R.J. (1974) Origin and Distribution of Ejecta from Near-Surface Laboratory Scale Cratering Experiments, University of Dayton Research Institute, to be published AFWL-TR-75, Air Force Weapons Lab.; Kirtland AFB, New Mexico.

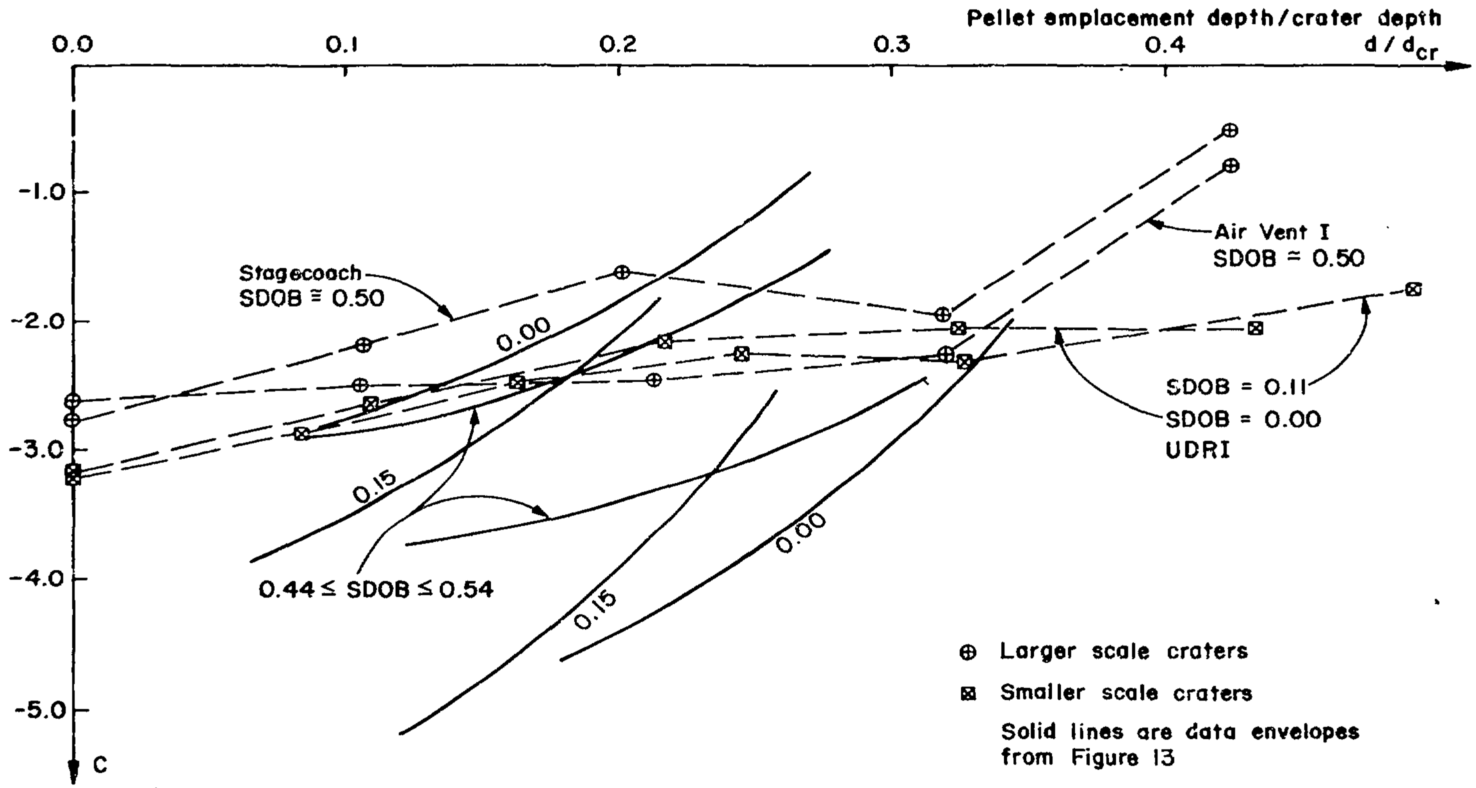

Figure 14. A Comparison of the Variation of the Exponent c [from Eq. (1)] with Depth Within the Ejecta Source Region for Explosion Experiments Conducted Over a Wide Range of Charge Size. Note that for the Stagecoach, Air Vent I, and UDRI experiments crater depth is measured from the original ground surface. Data trends from Figure 13 are also shown

particle size ≅ ejecta particle size] and the large-scale experiments (pellet-particle size ≅ limited fraction of ejecta-particle size) suggests that these results represent reasonable descriptions of the translation of the bulk of the crater ejecta. Thus, for explosion craters with shallow depths-of-burst ($0.00 \leq \text{SDOB} \leq 0.55$) in relatively unconsolidated geological materials, the translation of material ejected from the upper one-third to one-half of the crater of excavation can be approximately described by Eq. (1) in which the exponent $c = -2.5 \pm 1.0$.

On the other hand, the present study indicates that the coarsest fraction of the material ejected by explosive events with shallow SDOB travels to significantly greater ranges than finer-sized material originally situated in a similar preshot position. Essentially, this is a restatement of the general sorting effects of atmospheric drag on ejecta deposition: finer material is preferentially decelerated and deposited near the crater rim while the ballistic trajectories of larger fragments are relatively less affected by the atmosphere.[25] However, a comparison of the pellet-translation data of the present study with the ejecta-translation results of the larger and smaller scale experiments, permits a more quantitative description of the actual size-related differences in the translation of explosion crater ejecta. In particular, for shallow explosive events in relatively unconsolidated geological materials, the pellet-translation results presented here suggest that the translation of the coarsest fraction of near-surface ejecta may be approximately described by a power-law expression of the form of Eq. (1), in which the exponent $c = -4.0 \pm 1.0$. Furthermore, a maximum in the lateral translation of the coarsest size fraction of the ejected material may occur at a critical, near-surface SDOB. Such a maximum in the normalized translation range of the coarsest ejecta-size fractions would not appear to correspond to the SDOB which produces a maximum crater volume.

6. CONCLUSIONS AND IMPLICATIONS

(1) The excavation of explosion crater ejecta is a complicated process which consistently transports successively deeper levels of the target or test medium to successively smaller ranges beyond the crater rim. Postshot analysis of the distribution of emplaced pellets in large-scale 20-ton TNT experiments and the distribution of dyed-quartz sand tracer materials excavated by small-scale gram-sized explosive events indicate that the bulk of the ejected material originates from the upper portions of the crater. This material is excavated as a continuous sequence of nested spherical segments or shells as the crater grows. Furthermore, the lateral translation of the bulk of the material ejected by shallow explosive events ($0.00 < \text{SDOB} < 0.55$ ft/(lb TNT)$^{1/3}$) within poorly consolidated geological materials

(for example, sand and alluvium) is a surprisingly uniform phenomenon and can be empirically described by the expression:

$$\frac{r}{R} \propto \left(\frac{x}{R}\right)^{c} \text{ when } \begin{array}{c} c = -2.5 \pm 1.0 \\ \text{(bulk of the ejecta)} \end{array} .$$

The lateral translation of ejecta originating from the upper portions of the crater of excavation remains approximately constant for $0.00 < \text{SDOB} < 0.55$ ft/(lb TNT)$^{1/3}$ explosive events in poorly consolidated geological materials, whereas the crater depth/radius ratio increases by a factor of two with increasing SDOB.

Further experiments in a variety of softrock and hardrock materials would permit parametrization of the mapping exponent c for the bulk of the ejected material in terms of the physical properties of different earth media. Such a functional form for the mapping exponent could be used to quantitatively predict the postshot range of explosion crater ejecta as a function of its original position, the event SDOB, and the physical properties of the target or test medium.

(2) The coarsest fraction of explosion crater ejecta derived from unconsolidated geological materials will be translated to ranges which are much greater than the radial throwout distances which characterize finer-sized material initially situated in a similar preshot position. Values of c in the previous power-law expression, which describe the translation of this coarse-size fraction, lie in the range $c = -4.0 \pm 1.0$.

A comparison of the behavior of groups of artificial pellets emplaced within quartz sand demonstrates that (a) the translation of coarse material at near-surface levels is more highly variable than the translation of coarse material at intermediate levels for a particular type of event (that is, SDOB = constant), and (b) that with increasing SDOB, the translation of coarse material from near-surface levels is more strongly attenuated than the translation of coarse material originating at intermediate levels within the crater of excavation. These results imply that shallow bursts in poorly sorted unconsolidated geologic materials may eject significant amounts of blocky fragmental material well beyond the range of the continuous ejecta deposit. Further experiments in unconsolidated materials with different ranges of particle size would permit parametrization of the mapping exponent c for the coarsest ejecta-size fraction in terms of the degree of sorting of such materials.

(3) This study suggests that the lateral translation of coarser fractions of explosion-crater ejecta derived from unconsolidated geological materials may be maximized at a particular SDOB. Such a critical SDOB for the translation of the coarse-sized ejecta should not necessarily correspond to the SDOB producing maximum crater volume. The artificial pellets and quartz sand fill materials

suggest that this critical SDOB $\cong$ 0.15 $\pm$ 0.05 ft/(lb TNT)$^{1/3}$ for small explosive charges (1- to 10-lb TNT equivalent). Current understanding of the relationship between crater excavation and the process of ejecta deposition implies that the development of rays, and fragment chains and clusters within the zone of discontinuous deposition should be extensive for explosive events conducted at such a critical SDOB.

The threat that natural missiles pose to a nearby target surface is proportional to their size and velocity. Thus, a major conclusion of this study is that knowledge of the average translation of the bulk of the ejected material places a minimal constraint on the siting of "safe" surface structures. More realistic siting criteria should be based upon the translation of the coarser fractions of the explosion crater ejecta deposit.

(4) Models of ejecta translation can be combined with models of energy distribution and stress wave propagation in order to predict the post-event location of material which has experienced various degrees of shock metamorphism. This material can then be sampled directly within the ejecta deposit and its post-event strength and physical properties can be studied in the laboratory in detail. In turn, improved understanding of how specific shock stress histories change the measurable physical properties of geological materials will make it possible to employ individual ejecta samples as in-situ barometers which reflect transient stress conditions within the crater at the time of formation. Ultimately, knowledge of the initial stress distribution produced by the explosive event and the postshot distribution of stress-induced physical property changes in the ejected material will supply the quantitative boundary conditions required for a comprehensive model of ejecta translation.

(5) Caution is required in extrapolating the results of this study of explosion crater ejecta to the case of impact cratering. Oberbeck[17] and Baldwin[18] have demonstrated the similarity of crater dimensions, ejecta cloud growth, and subcrater deformation which can exist between craters formed by impact and craters formed by explosions within a limited range of SDOB. However, Oberbeck[17] has also demonstrated that projectile velocity critically influences impact crater dimensions and subsurface deformation. Projectile velocity may also critically influence the lateral translation of impact crater ejecta. The results of this study indicate that changes in the shape of explosion craters and the role of compressional deformation in crater formation do not severely change the observed translation of the bulk of the ejecta excavated by a variety of near-surface explosive cratering events. Since shallow SDOB events (SDOB = 0.25 $\pm$ 0.10 ft/(lb TNT)$^{1/3}$) provide an approximate analogy to the features of impact cratering mentioned above, this study tentatively supports the concept that the lateral translation of impact crater ejecta normalized to crater radius may be approximately uniform over a range of crater size and impact conditions even though impact and explosion cratering events are not identical phenomena.

References

1. Henny, R.W., and Carlson, R.H. (1970) Natural Missile Distributions for High Explosive Craters in Hard Rock, Vol. III, Multiple Threat Cratering Experiment, AFWL-TR-67-8, Air Force Weapons Lab., Kirtland AFB, New Mexico.

2. Strohberger, D.E. (1971) Mineral Rock Ejecta Study, Final Report, Contract DASA 01-70-C-0029, The Boeing Company, Seattle, Washington.

3. Linnerud, H.J. (1975) In-Flight Ejecta Size Distributions for Middle Gust III, Final Report, SAI-74-502-BN, Science Applications, Inc., Bedford, Massachusetts.

4. Sugge, R.L., and Stroberger, D.E. (1973) Transient Crater Ejecta Analysis, AFWL-TR-70-64, Air Force Weapons Lab., Kirtland AFB, Albuquerque, New Mexico.

5. Meyer, J.W., and Rooke, A.D. (1973) Operation Mine Shaft Distribution of Natural and Artificial Ejecta Resulting from Detonation of 100 ton TNT Charge on Granite, WES Misc. Paper N-73-4, U.S. Army Engineers Waterways Experiment Station, Vicksburg, Mississippi.

6. Dishon, J.F. (1974) Investigation of Intermediate and Maximum Range Missiles Produced by Cratering Experiments, MPE-74-2, U.S. Army Engineer Waterways Experimental Station, Explosive Excavation Res. Lab., Livermore, California.

7. Gault, D.E., Shoemaker, E.M., and Moore, H.J. (1963) Spray Ejected from the Lunar Surface by Meteoroid Impact, NASA-Tech Note D-1767, 39 pp.

8. Gault, D.E., Quaide, W.L., and Oberbeck, V.R. (1968) Impact cratering mechanics and structures, in Shock Metamorphism of Natural Materials, French, B.M. and Short, N.M. (eds.), The Mono Book Corp., Baltimore, Maryland.

9. Dence, M.R. (1968) Shock zoning at Canadian craters: Petrography and structural implications, in Shock Metamorphism of Natural Materials, French, B.M. and Short, N.M. (eds.), The Mono Book Corp., Baltimore, Maryland, pp 169-184.

10. Stoffler, D., Gault, D.E., Wedekind, J., and Polkowski, G. (1974) Experimental hypervelocity impact into quartz sand: Distribution and shock metamorphism of ejecta, Jour. Geophys. Res., submitted July 1974.

11. Oberbeck, V.R. (1975) The role of ballistic erosion and sedimentation in lunar stratigraphy, Reviews Geophys. Space Science 13:337-362.

12. McGetchin, T.R., Settle, M., and Head, J.W. (1973a) Radial thickness variation in impact crater ejecta: Implications for lunar basin deposits, Earth Planetary Sci. Lettr. 20:226-236.

13. Oberbeck, V.R., Morrison, R.H., Horz, F., Quaide, W.L., and Gault, D.E. (1974) Smooth Plains and Continuous Deposits of Craters and Basins, NASA Tech Mem X-62, 376, Ames Research Center, Moffett Field, California.

14. Oberbeck, V.R., Horz, F., Morrison, R.H., and Quaide, W.L. (1973) Emplacement of the Cayley Formation, NASA Tech Mem X-62, 302, Ames Research Center, Moffett Field, California.

15. Morrison, R.H., and Oberbeck, V.R. (1975) Features of crater continuous deposits and interpretations of their origin, Lunar Science VI, p. 578-580, The Lunar Science Institute, Houston, Texas.

16. Settle, M., and Head, J.W. (1975) Topographic variations in lunar crater rim profiles: Implications for the formation of ejecta deposits, submitted to Icarus.

17. Oberbeck, V.R. (1971) Laboratory simulation of impact cratering with high explosives, Jour. Geophys. Res. 76:5732-5749.

18. Baldwin, R.B. (1963) The Measure of the Moon, The University of Chicago Press, Chicago, Illinois.

19. Roberts, W.A. (1965) Permanent angular displacement and ejecta-induced impulse associated with crater formation, Icarus 4:480-493.

20. Settle, M., and Needleman, S. (1974) Deformation in granular earth media produced by explosive cratering: Implications for impact cratering, EOS Transactions Am. Geophys. Union 56, No. 12:1142.

21. Emerson, B.K. (1917) Geology of Massachusetts and Rhode Island, U.S. Geological Survey Bull. No. 597, 289 pp.

22. Durgunoglu, H.T. (1972) Static Penetration Resistance of Soils, PhD Thesis, University of California, Berkeley, California.

23. Turnage, G.W. (1974) Measuring Soil Properties in Vehicle Mobility Research; Resistance of Coarse Grained Soils to High Speed Penetration, Tech. Rpt No. 3-652, Report 6, U.S. Army Waterways Experiment Station, Mobility and Environmental Systems Lab., Vicksburg, Mississippi.

24. Fulmer, C.V. (1965) Cratering Characteristics of Wet and Dry Sand, The Boeing Company Report D2-90683-1, Seattle, Washington.

25. Sherwood, A.E. (1967) Effect of air drag on particles ejected during explosive cratering, Jour. Geophys. Res. 72:1783-1791.

26. Piekutowski, A.J. (1974) Laboratory Scale High Explosive Cratering and Ejecta Phenomenology Studies, University of Dayton Research Institute, AFWL-TR-72-155, Air Force Weapons Lab., Kirtland AFB, Albuquerque, New Mexico.

27. McGetchin, T.R., Settle, M., and Head, J.W. (1973b) A model for the distribution of impact crater ejecta and its implications, EOS Transactions Am. Geophys. Union 54, No. 4:357.

28. Nordyke, M.D. (1961) Nuclear craters and preliminary theory of the mechanics of explosive crater formation, Jour. Geophys. Res. 66:3439-3459.

29. Short, N.M. (1965) A comparison of features characteristic of nuclear explosion craters and astroblemes, Annals N.Y. Acad. Sci. 123:573-616.

30. Horz, F. (1969) Structural and mineralogical evaluation of an experimentally produced crater in granite, Contributions Mineralogy Petrology 21:365-377.

31. Ahlers, E.B. (1965) Crater Ejecta Studies - Flat Tops II and III, Project 1.5a, Ferris Wheel Series, Flat Top Event, POR - 3006, IIT Research Institute, Chicago, Illinois.

32. Anthony, M.V. (1965) Ejecta Distribution from the Flat Top I Event, Project 1.5b, Ferris Wheel Series, Flat Top Event, POR - 3007, The Boeing Company, Seattle, Washington.

33. Merritt, M.L. (1968) Ferris Wheel Series, Air Vent/Flat Top Events, Project Officers Report, Scientific Directors Summary, POR - 3000, Sandia Corporation, Albuquerque, New Mexico.

34. Dishon, J.F. (1975) ESSEX - Diamond Ore Research Program: Ejecta Measurements Report - ESSEX I, Phase I, WES MP-E-75-3, U.S. Army Waterways Experiment Station, Explosive Excavation Research Lab., Livermore, California.

35. Vortman, L.J., and MacDougall, H.R., eds. (1962) Project Stagecoach: 20 Ton HE Cratering Experiments in Desert Alluvium, Final Report, SC-4596, TID-4500, Sandia Corporation, Albuquerque, New Mexico.

36. Sun, J.M. (1970) Energy counter-pressure scaling equations of linear crater dimensions, Jour. Geophys. Res. 75:2003-2027.

37. White, J.W. (1973) An empirically derived cratering formula, Jour. Geophys. Res. 78:8623-8633.

38. Andrews, R.J. (1974) Origin and Distribution of Ejecta from Near-Surface Laboratory Scale Cratering Experiments, University of Dayton Research Institute, to be published AFWL-TR-75, Air Force Weapons Lab.; Kirtland AFB, New Mexico.

Appendix A

Field measurements of crater dimensions and pellet preshot and postshot ranges are presented in tabular form in this appendix. Table A1 serves as an index to the listing of the field data contained in Table A2. Table A1 can be used to identify the pellet groups employed in a specific experiment and provides data on pellet emplacement and the configuration of the explosive charge. Table A2 lists the preshot and postshot distances of individual pellets (measured from surface ground zero) and the results of a least-squares fit to the power-law expression discussed in this report [see Eq. (1)] for groups of pellets initially emplaced at a common depth beneath the original ground surface.

The explosion experiments are listed chronologically in both tables. In cases where incomplete or unreliable pellet data was returned from a specific experiment, it is not included in Table A2, although a description of pellet emplacement, charge configuration, and crater dimensions is provided in Table A1.

Guide to Table A1

DATE – date upon which the experiment was conducted.

EXPLOSIVE DOB (M) – explosive depth-of-burst (DOB), measured in meters from original ground surface to center of the explosive charge.

EXPLOSIVE TYPE – explosive material, see Table 2 in the text of this report.

EXPLOSIVE WT (LB) – explosive weight in pounds.

EQUIVALENT TNT WT (LB) – equivalent weight of a TNT charge in pounds, see Table 2 in the text of this report.

SCALED DOB – scaled depth-of-burst (SDOB) of the explosive charge determined by dividing actual charge depth-of-burst by the cube-root of the equivalent TNT charge weight (SDOB measured in ft/(lb TNT)$^{1/3}$).

Preceding page blank

PELLET DEPTH – depth of emplacement of a group of pellets measured from the original ground surface presented in centimeter and inch units.

PELLET TYPE – a description of the pellet material, see Table 1 in the text of this report (Al represents aluminum alloy pellets).

CRATER RAD (M) – crater rim crest radius measured in meters.

CRATER DEP (M) – crater depth measured from the rim crest in meters.

Guide to Table A2

Experiments are referenced by an identifier phrase which gives DEVENS as the experimental site followed by the experiment date, charge weight, approximate description of scaled depth-of-burst, pellet type, and pellet emplacement depth. Crater rim crest radii are presented in meters. The variable x refers to pre-shot pellet range; r refers to postshot pellet range (both measured from surface ground zero). A least-squares fit to the power-law expression discussed in the text [Eq. (1)] is presented beneath a tabular listing of the field measurements. (The first number after the = sign is a multiplicative factor; the second number represents the exponent c in the power law expression.) The correlation coefficient represents a measure of goodness-of-fit; a value of 1.000 is indicative of an 'exact' fitting of the data.

Table A1. Index to the Listing of Field Data in Table A2

DATE	EXPLOSIVE DEPTH(M)	EXPLOSIVE TYPE	EXPLOSIVE WT(LBS)	EQUIVALENT TNT WT(LBS)	SCALED DOB	PELLET DEPTH(CM)	PELLET DEPTH(IN)	PELLET TYPE	CRATER RADIUS(M)	CRATER DEPTH(M)
1OCT73	0.000	HI-VEL	5.000	4.250	0.000	5.08	2.00	GREEN GLASS	.841	.287
1OCT73	0.000	HI-VEL	5.000	4.250	0.000	7.62	3.00	GREEN GLASS	.841	.287
1OCT73	0.000	HI-VEL	5.000	4.250	0.000	5.08	2.00	ORANGE ACRYLIC	.841	.287
1OCT73	0.000	HI-VEL	5.000	4.250	0.000	7.62	3.00	ORANGE ACRYLIC	.841	.287
1OCT73	0.000	HI-VEL	5.000	4.250	0.000	10.16	4.00	ORANGE ACRYLIC	.841	.287
10OCT73	0.000	HI-VEL	10.000	8.500	0.000	2.54	1.00	GREEN GLASS	1.012	.381
10OCT73	0.000	HI-VEL	10.000	8.500	0.000	5.08	2.00	GREEN GLASS	1.012	.381
10OCT73	0.000	HI-VEL	10.000	8.500	0.000	7.62	3.00	GREEN GLASS	1.012	.381
10OCT73	0.000	HI-VEL	10.000	8.500	0.000	2.54	1.00	ORANGE ACRYLIC	1.012	.381
10OCT73	0.000	HI-VEL	10.000	8.500	0.000	5.08	2.00	ORANGE ACRYLIC	1.012	.381
10OCT73	0.000	HI-VEL	10.000	8.500	0.000	7.62	3.00	ORANGE ACRYLIC	1.012	.381
11OCT73	.044	HI-VEL	1.000	.850	.151	2.54	1.00	RED ACRYLIC	.622	.235
11OCT73	.044	HI-VEL	1.000	.850	.151	5.08	2.00	ORANGE ACRYLIC	.622	.235
11OCT73	.044	HI-VEL	1.000	.850	.151	2.54	1.00	GREEN GLASS	.622	.235
11OCT73	.055	HI-VEL	2.000	1.700	.150	2.54	1.00	RED ACRYLIC	.841	.274
11OCT73	.055	HI-VEL	2.000	1.700	.150	5.08	2.00	ORANGE ACRYLIC	.841	.274
11OCT73	.055	HI-VEL	2.000	1.700	.150	2.54	1.00	GREEN GLASS	.841	.274
11OCT73	0.000	HI-VEL	3.000	2.550	0.000	2.54	1.00	RED ACRYLIC	.738	.247
11OCT73	0.000	HI-VEL	3.000	2.550	0.000	5.08	2.00	ORANGE ACRYLIC	.738	.247
11OCT73	0.000	HI-VEL	3.000	2.550	0.000	2.54	1.00	GREEN GLASS	.738	.247
11OCT73	0.000	HI-VEL	4.000	3.400	0.000	2.54	1.00	RED ACRYLIC	.792	.247
11OCT73	0.000	HI-VEL	4.000	3.400	0.000	5.08	2.00	ORANGE ACRYLIC	.792	.247
11OCT73	0.000	HI-VEL	4.000	3.400	0.000	2.54	1.00	GREEN GLASS	.792	.247
16OCT73	0.000	HI-VEL	1.000	.850	0.000	2.54	1.00	RED ACRYLIC	.561	.177
16OCT73	0.000	HI-VEL	1.000	.850	0.000	5.08	2.00	ORANGE ACRYLIC	.561	.177
16OCT73	0.000	HI-VEL	1.000	.850	0.000	2.54	1.00	GREEN GLASS	.561	.177
16OCT73	0.000	HI-VEL	2.000	1.700	0.000	2.54	1.00	RED ACRYLIC	.719	.213
16OCT73	0.000	HI-VEL	2.000	1.700	0.000	5.08	2.00	ORANGE ACRYLIC	.719	.213
16OCT73	0.000	HI-VEL	2.000	1.700	0.000	7.62	3.00	GREEN GLASS	.719	.213
16OCT73	.062	HI-VEL	3.000	2.550	.149	2.54	1.00	RED ACRYLIC	.914	.280
16OCT73	.062	HI-VEL	3.000	2.550	.149	5.08	2.00	ORANGE ACRYLIC	.914	.280
16OCT73	.062	HI-VEL	3.000	2.550	.149	2.54	1.00	GREEN GLASS	.914	.280
16OCT73	.069	HI-VEL	4.000	3.400	.150	2.54	1.00	RED ACRYLIC	1.012	.381
16OCT73	.069	HI-VEL	4.000	3.400	.150	5.08	2.00	ORANGE ACRYLIC	1.012	.381
16OCT73	.069	HI-VEL	4.000	3.400	.150	2.54	1.00	GREEN GLASS	1.012	.381
16OCT73	.055	HI-VEL	2.000	1.700	.150	2.54	1.00	RED ACRYLIC	.704	.259
16OCT73	.055	HI-VEL	2.000	1.700	.150	5.08	2.00	ORANGE ACRYLIC	.704	.259
16OCT73	.055	HI-VEL	2.000	1.700	.150	2.54	1.00	GREEN GLASS	.704	.259
3APR74	.184	HI-VEL	5.000	4.250	.211	5.08	2.00	RED ACRYLIC	1.024	.439
3APR74	.184	HI-VEL	5.000	4.250	.211	7.62	3.00	ORANGE ACRYLIC	1.024	.439
3APR74	.184	HI-VEL	5.000	4.250	.211	5.08	2.00	YELLOW GLASS	1.024	.439
3APR74	.208	HI-VEL	5.000	4.250	.422	5.08	2.00	RED ACRYLIC	1.183	.527
3APR74	.208	HI-VEL	5.000	4.250	.422	7.62	3.00	ORANGE ACRYLIC	1.183	.527
3APR74	.208	HI-VEL	5.000	4.250	.422	5.08	2.00	YELLOW GLASS	1.183	.527
3APR74	.264	HI-VEL	5.000	4.250	.536	5.08	2.00	YELLOW GLASS	1.280	.686
6JUNE74	.264	HI-VEL	5.000	4.250	.536	5.08	2.00	RED ACRYLIC	1.259	.710
6JUNE74	.264	HI-VEL	5.000	4.250	.536	5.08	2.00	BLUE GLASS	1.259	.710
6JUNE74	[illegible]	HI-VEL	5.000	4.250	[illegible]	5.08	2.00	BROWN GLASS	1.080	.415
19JULY74	0.000	HI-VEL	5.000	4.250	0.000	2.54	1.00	RED ACRYLIC	.518	.171
19JULY74	0.000	HI-VEL	5.000	4.250	0.000	2.54	1.00	BROWN GLASS	.518	.171
19JULY74	0.000	HI-VEL	5.000	4.250	0.000	5.08	2.00	BLUE GLASS	.518	.171
19JULY74	0.000	HI-VEL	5.000	4.250	0.000	2.54	1.00	AL	.518	.171
19JULY74	0.000	HI-VEL	5.000	4.250	0.000	5.08	2.00	AL	.518	.171
31JULY74	.055	HI-VEL	.380	.323	.262	2.54	1.00	ORANGE ACRYLIC	.622	.241
31JULY74	.055	HI-VEL	.380	.323	.262	5.08	2.00	RED ACRYLIC	.622	.241
31JULY74	.055	HI-VEL	.380	.323	.262	2.54	1.00	BLUE GLASS	.622	.241
31JULY74	.055	HI-VEL	.380	.323	.262	5.08	2.00	BROWN GLASS	.622	.241
31JULY74	.055	HI-VEL	.380	.323	.262	2.54	1.00	AL	.622	.241
31JULY74	.055	HI-VEL	.380	.323	.262	5.08	2.00	AL	.622	.241
31JULY74	.055	HI-VEL	.380	.323	.262	7.62	3.00	AL	.622	.241
18SEPT74	0.000	C4	1.000	1.300	0.000	2.54	1.00	AL	.658	.329
18SEPT74	0.000	C4	1.000	1.300	0.000	7.62	3.00	AL	.658	.329
18SEPT74	0.000	C4	1.000	1.300	0.000	11.43	4.50	AL	.658	.329
18SEPT74	.076	C4	1.000	1.300	.229	2.54	1.00	AL	.713	.317
18SEPT74	.076	C4	1.000	1.300	.229	7.62	3.00	AL	.713	.317
18SEPT74	.076	C4	1.000	1.300	.229	11.43	4.50	AL	.713	.317
18SEPT74	.152	C4	1.000	1.300	.458	2.54	1.00	AL	.841	.451
18SEPT74	.152	C4	1.000	1.300	.458	7.62	3.00	AL	.841	.451
18SEPT74	.152	C4	1.000	1.300	.458	11.43	4.50	AL	.841	.451
18SEPT74	.114	C4	1.000	1.300	.344	2.54	1.00	AL	.799	.329
18SEPT74	.114	C4	1.000	1.300	.344	7.62	3.00	AL	.799	.329
18SEPT74	.114	C4	1.000	1.300	.344	12.70	5.00	AL	.799	.329
25SEPT74	0.000	C4	1.100	1.430	0.000	2.54	1.00	AL	.652	.305
25SEPT74	0.000	C4	1.100	1.430	0.000	5.08	2.00	AL	.652	.305
25SEPT74	.076	C4	1.100	1.430	.222	2.54	1.00	AL	.759	.302
25SEPT74	.076	C4	1.100	1.430	.222	5.08	2.00	AL	.759	.302
25SEPT74	.076	C4	1.100	1.430	.222	7.62	3.00	AL	.759	.302
25SEPT74	.152	C4	1.100	1.430	.444	5.08	2.00	AL	.866	.369
25SEPT74	.152	C4	1.100	1.430	.444	7.62	3.00	AL	.866	.369
25SEPT74	.152	C4	1.100	1.430	.444	10.16	4.00	AL	.866	.369

Table A2. Preshot and Postshot Distances of Individual Pellets

DEVENS 10OCT7315LB,HALF-BURIED:GREEN GLASS,2 INCH — CRATER RADIUS(RC)= .841 METERS
PELLET DEPTH OF BURIAL = 5.08CM

FIELD DATA:	----PRESHOT PELLET RANGES---- X METERS	X/RC	LOG10(X/RC)	----POSTSHOT PELLET RANGES---- R METERS	R/RC	LOG10(R/RC)
	.305	.3623	-.44091	23.997	28.5296	1.45523
	.381	.4529	-.34400	5.395	6.4138	.80706
	.457	.5435	-.26482	1.402	1.6667	.22185
	.533	.6341	-.19787	1.588	1.8877	.27593
	.610	.7254	-.13980	1.378	1.6377	.21423

LST SQ FIT TO LOG-LOG EQUATION (R/RC)= .270*(X/RC)** -4.194 CORRELATION COEFFICIENT= .9217

DEVENS 10OCT7315LB,HALF-BURIED:GREEN GLASS,3 INCH — CRATER RADIUS(RC)= .841 METERS
PELLET DEPTH OF BURIAL = 7.62CM

FIELD DATA:	----PRESHOT PELLET RANGES---- X METERS	X/RC	LOG10(X/RC)	----POSTSHOT PELLET RANGES---- R METERS	R/RC	LOG10(R/RC)
	.305	.3623	-.44091	2.505	2.9783	.47396
	.381	.4529	-.34400	2.368	2.8152	.44951
	.457	.5435	-.26482	1.396	1.6596	.21996

LST SQ FIT TO LOG-LOG EQUATION (R/RC)= .775*(X/RC)** -1.399 CORRELATION COEFFICIENT= .6883

DEVENS 10OCT7315LB,HALF-BURIED:ORANGE ACRYLIC,2INCH — CRATER RADIUS(RC)= .841 METERS
PELLET DEPTH OF BURIAL = 5.08CM

FIELD DATA:	----PRESHOT PELLET RANGES---- X METERS	X/RC	LOG10(X/RC)	----POSTSHOT PELLET RANGES---- R METERS	R/RC	LOG10(R/RC)
	.305	.3623	-.44091	13.777	16.3768	1.21423
	.381	.4529	-.34400	4.292	5.1014	.70769
	.457	.5435	-.26482	1.869	2.2210	.34659
	.533	.6341	-.19787	1.045	1.2426	.09439

LST SQ FIT TO LOG-LOG EQUATION (R/RC)= .140*(X/RC)** -4.630 CORRELATION COEFFICIENT= .9976

DEVENS 10OCT7315LB,HALF-BURIED:ORANGE ACRYLIC,3 INCH — CRATER RADIUS(RC)= .841 METERS
PELLET DEPTH OF BURIAL = 7.62CM

FIELD DATA:	----PRESHOT PELLET RANGES---- X METERS	X/RC	LOG10(X/RC)	----POSTSHOT PELLET RANGES---- R METERS	R/RC	LOG10(R/RC)
	.305	.3623	-.44091	3.163	3.7609	.57529
	.381	.4529	-.34400	1.286	1.5290	.18440
	.457	.5435	-.26482	1.189	1.4138	.15018

LST SQ FIT TO LOG-LOG EQUATION (R/RC)= .276*(X/RC)** -2.676 CORRELATION COEFFICIENT= .9230

DEVENS 10OCT7315LB,HALF-BURIED:ORANGE ACRYLIC,4 INCH — CRATER RADIUS(RC)= .841 METERS
PELLET DEPTH OF BURIAL = 7.62CM

FIELD DATA:	----PRESHOT PELLET RANGES---- X METERS	X/RC	LOG10(X/RC)	----POSTSHOT PELLET RANGES---- R METERS	R/RC	LOG10(R/RC)
	.305	.3623	-.44091	1.817	2.1596	.33436
	.381	.4529	-.34400	1.170	1.3913	.14342

LST SQ FIT TO LOG-LOG EQUATION (R/RC)= .292*(X/RC)** -1.970 CORRELATION COEFFICIENT= 1.0000

DEVENS 10OCT73I10LB,HALF-BURIED:GREEN GLASS,1 INCH — CRATER RADIUS(RC)=1.011 METERS
PELLET DEPTH OF BURIAL = 2.54CM

FIELD DATA:	----PRESHOT PELLET RANGES---- X METERS	X/RC	LOG10(X/RC)	----POSTSHOT PELLET RANGES---- R METERS	R/RC	LOG10(R/RC)
	.381	.3767	-.42397	39.466	39.0375	1.59133
	.457	.4521	-.34479	23.314	23.0530	1.36273
	.533	.5274	-.27786	13.786	13.6317	1.13459
	.610	.6028	-.21985	9.104	9.0024	.95436
	.686	.6781	-.16869	4.862	4.8071	.68188
	.762	.7535	-.12296	1.701	1.6817	.22576

LST SQ FIT TO LOG-LOG EQUATION (R/RC)= .782*(X/RC)** -4.231 CORRELATION COEFFICIENT= .9698

DEVENS 10OCT73I10LB,HALF-BURIED:GREEN GLASS,2 INCH — CRATER RADIUS(RC)=1.011 METERS
PELLET DEPTH OF BURIAL = 5.08CM

FIELD DATA:	----PRESHOT PELLET RANGES---- X METERS	X/RC	LOG10(X/RC)	----POSTSHOT PELLET RANGES---- R METERS	R/RC	LOG10(R/RC)
	.457	.4521	-.34479	10.415	10.3014	1.01290
	.533	.5274	-.27786	5.471	5.4099	.73319
	.610	.6028	-.21985	1.946	1.9241	.28379
	.686	.6781	-.16869	1.722	1.7028	.23117

LST SQ FIT TO LOG-LOG EQUATION (R/RC)= .380*(X/RC)** -4.286 CORRELATION COEFFICIENT= .9811

Table A2. Preshot and Postshot Distances of Individual Pellets (Cont)

DEVENS 10OCT73110LB,HALF-BURIED:GREEN GLASS,3 INCH CRATER RADIUS(RC)=1.011 METERS
PELLET DEPTH OF BURIAL = 7.62CM

FIELD DATA:	----PRESHOT PELLET RANGES-----			----POSTSHOT PELLET RANGES----		
	X METERS	X/RC	LOG10(X/RC)	R METERS	R/RC	LOG10(R/RC)
	.229	.2265	-.64582	19.266	19.0566	1.27991
	.305	.3016	-.52088	14.402	14.2445	1.15351
	.381	.3767	-.42397	7.530	7.4477	.87239
	.457	.4521	-.34479	3.100	3.0651	.48644
	.533	.5276	-.27786	2.347	2.3207	.36561
	.610	.6028	-.21985	1.951	1.9289	.28533

LST SQ FIT TO LOG-LOG EQUATION (R/RC)= .494*(X/RC)** -2.692 CORRELATION COEFFICIENT= .9779

DEVENS 10OCT73110LB,HALF-BURIED:ORANGE ACRYLIC,1 INCH CRATER RADIUS(RC)=1.011 METERS
PELLET DEPTH OF BURIAL = 2.54CM

FIELD DATA:	----PRESHOT PELLET RANGES-----			----POSTSHOT PELLET RANGES----		
	X METERS	X/RC	LOG10(X/RC)	R METERS	R/RC	LOG10(R/RC)
	.305	.3016	-.52088	18.715	18.5051	1.26729
	.381	.3767	-.42397	16.703	16.5150	1.21790
	.457	.4521	-.34479	12.567	12.4262	1.09434
	.533	.5276	-.27786	10.025	9.9126	.99619
	.610	.6028	-.21985	5.736	5.6721	.75374
	.686	.6781	-.16869	3.901	3.8577	.58633
	.762	.7535	-.12296	1.676	1.6576	.21949
	.838	.8288	-.08154	1.149	1.1357	.05546

LST SQ FIT TO LOG-LOG EQUATION (R/RC)= 1.039*(X/RC)** -2.836 CORRELATION COEFFICIENT= .9371

DEVENS 10OCT73110LB,HALF-BURIED:ORANGE ACRYLIC,2 INCH CRATER RADIUS(RC)=1.011 METERS
PELLET DEPTH OF BURIAL = 5.08CM

FIELD DATA:	----PRESHOT PELLET RANGES-----			----POSTSHOT PELLET RANGES----		
	X METERS	X/RC	LOG10(X/RC)	R METERS	R/RC	LOG10(R/RC)
	.305	.3016	-.52088	17.684	17.4866	1.24279
	.381	.3767	-.42397	9.095	8.9996	.95426
	.457	.4521	-.34479	7.489	7.4051	.86953
	.533	.5276	-.27786	4.266	4.2196	.62525
	.610	.6028	-.21985	3.946	3.9030	.59139
	.686	.6781	-.16869	2.216	2.1911	.34066
	.762	.7535	-.12296	1.274	1.2598	.10039

LST SQ FIT TO LOG-LOG EQUATION (R/RC)= .752*(X/RC)** -2.618 CORRELATION COEFFICIENT= .9768

DEVENS 10OCT73110LB,HALF-BURIED:ORANGE ACRYLIC,3 INCH CRATER RADIUS(RC)=1.011 METERS
PELLET DEPTH OF BURIAL = 7.62CM

FIELD DATA:	----PRESHOT PELLET RANGES-----			----POSTSHOT PELLET RANGES----		
	X METERS	X/RC	LOG10(X/RC)	R METERS	R/RC	LOG10(R/RC)
	.229	.2265	-.64582	11.825	11.6958	1.06796
	.305	.3016	-.52088	6.852	6.7752	.83092
	.381	.3767	-.42397	2.993	2.9596	.47124
	.533	.5276	-.27786	2.155	2.1309	.32856
	.610	.6028	-.21985	1.091	1.0786	.03287

LST SQ FIT TO LOG-LOG EQUATION (R/RC)= .361*(X/RC)** -2.356 CORRELATION COEFFICIENT= .9796

DEVENS 11OCT73111LB,FULL BURIED:RED ACRYLIC,1 INCH CRATER RADIUS(RC)= .622 METERS
PELLET DEPTH OF BURIAL = 2.54CM

FIELD DATA:	----PRESHOT PELLET RANGES-----			----POSTSHOT PELLET RANGES----		
	X METERS	X/RC	LOG10(X/RC)	R METERS	R/RC	LOG10(R/RC)
	.152	.2449	-.61109	15.901	25.5645	1.40737
	.229	.3673	-.43499	6.109	11.0266	1.11681
	.305	.4897	-.31006	1.111	1.7875	.25224
	.381	.6121	-.21315	.935	1.4565	.16272

LST SQ FIT TO LOG-LOG EQUATION (R/RC)= .260*(X/RC)** -1.451 CORRELATION COEFFICIENT= .9546

DEVENS 11OCT73111LB,FULL BURIED:ORANGE ACRYLIC,2 INCH CRATER RADIUS(RC)= .622 METERS
PELLET DEPTH OF BURIAL = 5.08CM

FIELD DATA:	----PRESHOT PELLET RANGES-----			----POSTSHOT PELLET RANGES----		
	X METERS	X/RC	LOG10(X/RC)	R METERS	R/RC	LOG10(R/RC)
	.152	.2449	-.61109	9.585	15.4016	1.18758
	.229	.3673	-.43499	4.770	7.6661	.88446
	.305	.4897	-.31006	1.353	2.1743	.33733

LST SQ FIT TO LOG-LOG EQUATION (R/RC)= .362*(X/RC)** -2.792 CORRELATION COEFFICIENT= .9699

Table A2. Preshot and Postshot Distances of Individual Pellets (Cont)

DEVENS 11OCT7311LB,FULL BURIED:GREEN GLASS,1 INCH CRATER RADIUS(RC)= .622 METERS
PELLET DEPTH OF BURIAL = 2.54CM

FIELD DATA:	----PRESHOT PELLET RANGES----- X METERS	X/RC	LOG10(X/RC)	----POSTSHOT PELLET RANGES---- R METERS	R/RC	LOG10(R/RC)
	.152	.2449	-.61109	24.613	39.5446	1.59709
	.229	.3673	-.43499	9.982	16.0382	1.20516
	.305	.4897	-.31006	4.008	6.4398	.80887
	.381	.6121	-.21315	.899	1.4447	.15977

LST SQ FIT TO LOG-LOG EQUATION (R/RC)= .388*(X/RC)** -3.492 CORRELATION COEFFICIENT= .9871

DEVENS 11OCT7312LB,FULL BURIED:RED ACRYLIC,1 INCH CRATER RADIUS(RC)= .841 METERS
PELLET DEPTH OF BURIAL = 2.54CM

FIELD DATA:	----PRESHOT PELLET RANGES----- X METERS	X/RC	LOG10(X/RC)	----POSTSHOT PELLET RANGES---- R METERS	R/RC	LOG10(R/RC)
	.305	.3623	-.44091	48.615	57.7899	1.76185
	.381	.4529	-.34400	25.908	30.7971	1.48851
	.457	.5435	-.26482	12.040	14.3116	1.15569
	.533	.6341	-.19782	2.448	2.9099	.46381
	.610	.7246	-.13988	1.052	1.2500	.09691

LST SQ FIT TO LOG-LOG EQUATION (R/RC)= .255*(X/RC)** -5.692 CORRELATION COEFFICIENT= .9704

DEVENS 11OCT7312LB,FULL BURIED:LOOSE SAND ACRYLIC,2 INCH CRATER RADIUS(RC)= .841 METERS
PELLET DEPTH OF BURIAL = 5.08CM

FIELD DATA:	----PRESHOT PELLET RANGES----- X METERS	X/RC	LOG10(X/RC)	----POSTSHOT PELLET RANGES---- R METERS	R/RC	LOG10(R/RC)
	.229	.2717	-.56585	38.984	46.3406	1.66596
	.305	.3623	-.44091	16.734	19.8913	1.29866
	.381	.4529	-.34400	8.321	9.8913	.99525
	.457	.5435	-.26482	3.231	3.8406	.58440

LST SQ FIT TO LOG-LOG EQUATION (R/RC)= .526*(X/RC)** -3.503 CORRELATION COEFFICIENT= .9909

DEVENS 11OCT7312LB,FULL BURIED:GREEN GLASS,1 INCH CRATER RADIUS(RC)= .841 METERS
PELLET DEPTH OF BURIAL = 2.54CM

FIELD DATA:	----PRESHOT PELLET RANGES----- X METERS	X/RC	LOG10(X/RC)	----POSTSHOT PELLET RANGES---- R METERS	R/RC	LOG10(R/RC)
	.305	.3623	-.44091	56.937	67.6812	1.83047
	.381	.4529	-.34400	22.144	26.3225	1.42033
	.457	.5435	-.26482	7.226	8.5870	.93384
	.533	.6341	-.19782	4.054	4.8188	.68294
	.610	.7246	-.13988	1.875	2.2281	.34797

LST SQ FIT TO LOG-LOG EQUATION (R/RC)= .470*(X/RC)** -6.941 CORRELATION COEFFICIENT= .9977

DEVENS 11OCT7313LB,HALF-BURIED:RED ACRYLIC,1 INCH CRATER RADIUS(RC)= .737 METERS
PELLET DEPTH OF BURIAL = 2.54CM

FIELD DATA:	----PRESHOT PELLET RANGES----- X METERS	X/RC	LOG10(X/RC)	----POSTSHOT PELLET RANGES---- R METERS	R/RC	LOG10(R/RC)
	.152	.2069	-.68431	45.461	61.7087	1.79035
	.229	.3103	-.50822	21.717	29.4787	1.46951
	.305	.4137	-.38328	8.733	11.8535	1.07385
	.381	.5172	-.28637	4.923	6.6818	.82490
	.457	.6206	-.20719	1.494	2.0273	.30692
	.533	.7240	-.14026	.975	1.3240	.12187
	.610	.8275	-.08225	.792	1.0757	.03170

LST SQ FIT TO LOG-LOG EQUATION (R/RC)= .593*(X/RC)** -3.146 CORRELATION COEFFICIENT= .9852

DEVENS 11OCT7313LB,HALF-BURIED:SAND ACRYLIC,2 INCH CRATER RADIUS(RC)= .737 METERS
PELLET DEPTH OF BURIAL = 5.08CM

FIELD DATA:	----PRESHOT PELLET RANGES----- X METERS	X/RC	LOG10(X/RC)	----POSTSHOT PELLET RANGES---- R METERS	R/RC	LOG10(R/RC)
	.152	.2069	-.68431	22.647	30.7406	1.48771
	.229	.3103	-.50822	3.700	4.0939	.55875
	.305	.4137	-.38328	2.402	3.2602	.51325
	.381	.5172	-.28637	1.335	1.8122	.25820
	.457	.6205	-.20719	1.356	1.8411	.26508
	.533	.7240	-.14026	.756	1.0261	.01118

LST SQ FIT TO LOG-LOG EQUATION (R/RC)= .397*(X/RC)** -2.670 CORRELATION COEFFICIENT= .9862

Table A2. Preshot and Postshot Distances of Individual Pellets (Cont)

DEVENS 11OCT7313LB,HALF-BURIED:GREEN GLASS,1 INCH CRATER RADIUS(RC)= .737 METERS
PELLET DEPTH OF BURIAL = 2.54CM

FIELD DATA:	----PRESHOT PELLET RANGES-----			----POSTSHOT PELLET RANGES----		
	X METERS	X/RC	LOG10(X/RC)	R METERS	R/RC	LOG10(R/RC)
	.229	.3103	-.50822	21.010	28.5108	1.45513
	.305	.4137	-.38328	7.727	10.4882	1.02070
	.381	.5172	-.28637	6.538	8.8746	.94819
	.457	.6206	-.20719	1.716	2.3293	.36723
	.533	.7240	-.14024	1.143	1.5515	.19075
	.610	.8275	-.08225	.853	1.1585	.06388

LST SQ FIT TO LOG-LOG EQUATION (R/RC)= .584*(X/RC)** -3.368 CORRELATION COEFFICIENT= .9795

DEVENS 11OCT7314LB,HALF-BURIED:RED ACRYLIC,1 INCH CRATER RADIUS(RC)= .796 METERS
PELLET DEPTH OF BURIAL = 2.54CM

FIELD DATA:	----PRESHOT PELLET RANGES-----			----POSTSHOT PELLET RANGES----		
	X METERS	X/RC	LOG10(X/RC)	R METERS	R/RC	LOG10(R/RC)
	.229	.2880	-.54058	31.929	40.2266	1.60451
	.305	.3840	-.41566	17.578	22.1467	1.34531
	.381	.4800	-.31873	3.044	3.8402	.58436
	.457	.5760	-.23955	3.369	4.2445	.62772
	.533	.6720	-.17260	1.082	1.3631	.13459
	.610	.7680	-.11461	.905	1.1406	.05712

LST SQ FIT TO LOG-LOG EQUATION (R/RC)= .369*(X/RC)** -1.858 CORRELATION COEFFICIENT= .9722

DEVENS 11OCT7314LB,HALF-BURIED:ORANGE ACRYLIC,2 INCH CRATER RADIUS(RC)= .796 METERS
PELLET DEPTH OF BURIAL = 5.08CM

FIELD DATA:	----PRESHOT PELLET RANGES-----			----POSTSHOT PELLET RANGES----		
	X METERS	X/RC	LOG10(X/RC)	R METERS	R/RC	LOG10(R/RC)
	.152	.1920	-.71667	33.132	41.7435	1.62059
	.229	.2880	-.54058	18.258	23.0031	1.36179
	.305	.3840	-.41566	4.401	5.5453	.74393
	.381	.4800	-.31873	1.530	1.9278	.28506
	.457	.5760	-.23955	.960	1.2097	.08267

LST SQ FIT TO LOG-LOG EQUATION (R/RC)= .189*(X/RC)** -3.454 CORRELATION COEFFICIENT= .9786

DEVENS 11OCT7314LB,HALF-BURIED:GREEN GLASS,1 INCH CRATER RADIUS(RC)= .796 METERS
PELLET DEPTH OF BURIAL = 2.54CM

FIELD DATA:	----PRESHOT PELLET RANGES-----			----POSTSHOT PELLET RANGES----		
	X METERS	X/RC	LOG10(X/RC)	R METERS	R/RC	LOG10(R/RC)
	.229	.2880	-.54058	38.655	48.7020	1.68755
	.305	.3840	-.41566	8.067	10.1382	1.00595
	.381	.4800	-.31873	2.806	3.5330	.54815
	.457	.5760	-.23955	2.240	2.8226	.45069
	.533	.6720	-.17260	1.341	1.6897	.22781
	.610	.7680	-.11461	.899	1.1329	.05418

LST SQ FIT TO LOG-LOG EQUATION (R/RC)= .357*(X/RC)** -3.698 CORRELATION COEFFICIENT= .9812

DEVENS 16OCT7311LB,HALF-BURIED:RED ACRYLIC,1 INCH CRATER RADIUS(RC)= .562 METERS
PELLET DEPTH OF BURIAL = 2.54CM

FIELD DATA:	----PRESHOT PELLET RANGES-----			----POSTSHOT PELLET RANGES----		
	X METERS	X/RC	LOG10(X/RC)	R METERS	R/RC	LOG10(R/RC)
	.152	.2711	-.56679	39.673	70.5803	1.84869
	.229	.4077	-.38978	9.132	16.2479	1.21078
	.305	.5423	-.26576	1.651	2.9391	.46824
	.381	.6779	-.16885	.616	1.0956	.03959

LST SQ FIT TO LOG-LOG EQUATION (R/RC)= .190*(X/RC)** -4.636 CORRELATION COEFFICIENT= .9947

DEVENS 16OCT7311LB,HALF-BURIED:ORANGE ACRYLIC,2 INCH CRATER RADIUS(RC)= .562 METERS
PELLET DEPTH OF BURIAL = 5.08CM

FIELD DATA:	----PRESHOT PELLET RANGES-----			----POSTSHOT PELLET RANGES----		
	X METERS	X/RC	LOG10(X/RC)	R METERS	R/RC	LOG10(R/RC)
	.152	.2711	-.56679	4.517	8.0369	.90508
	.229	.4077	-.38978	1.699	3.0208	.48009
	.305	.5423	-.26576	1.091	1.9416	.28812
	.381	.6779	-.16885	.646	1.1497	.06057

LST SQ FIT TO LOG-LOG EQUATION (R/RC)= .514*(X/RC)** -2.077 CORRELATION COEFFICIENT= .9969

Table A2. Preshot and Postshot Distances of Individual Pellets (Cont)

DEVENS 16OCT73:1LB,HALF-BURIED:GREEN GLASS,1 INCH   CRATER RADIUS(RC)= .562 METERS
PELLET DEPTH OF BURIAL = 2.54CM

FIELD DATA:	----PRESHOT PELLET RANGES-----			----POSTSHOT PELLET RANGES----		
	X METERS	X/RC	LOG10(X/RC)	R METERS	R/RC	LOG10(R/RC)
	.152	.2711	-.56679	21.580	38.3948	1.58427
	.229	.4067	-.39070	8.111	14.4306	1.15928
	.305	.5423	-.26576	3.859	6.8655	.83667

LST SQ FIT TO LOG-LOG EQUATION (R/RC)= 1.523*(X/RC)** -2.479 CORRELATION COEFFICIENT= .9998

DEVENS 16OCT73:2LB,HALF-BURIED:RED ACRYLIC,1 INCH   CRATER RADIUS(RC)= .719 METERS
PELLET DEPTH OF BURIAL = 2.54CM

FIELD DATA:	----PRESHOT PELLET RANGES-----			----POSTSHOT PELLET RANGES----		
	X METERS	X/RC	LOG10(X/RC)	R METERS	R/RC	LOG10(R/RC)
	.229	.3181	-.49748	20.[illegible]	28.9779	1.46207
	.305	.4241	-.37254	10.363	14.4190	1.15894
	.381	.5301	-.27563	4.679	6.5098	.81356
	.457	.6361	-.19645	2.597	3.6132	.55790
	.533	.7422	-.12951	1.113	1.5479	.18975

LST SQ FIT TO LOG-LOG EQUATION (R/RC)= .689*(X/RC)** -3.392 CORRELATION COEFFICIENT= .9901

DEVENS 16OCT73:2LB,HALF-BURIED:ORANGE ACRYLIC,2 INCH   CRATER RADIUS(RC)= .719 METERS
PELLET DEPTH OF BURIAL = 5.08CM

FIELD DATA:	----PRESHOT PELLET RANGES-----			----POSTSHOT PELLET RANGES----		
	X METERS	X/RC	LOG10(X/RC)	R METERS	R/RC	LOG10(R/RC)
	.152	.2120	-.67357	2.015	2.8032	.44766
	.229	.3181	-.49748	1.926	2.6802	.42817
	.305	.4241	-.37254	1.509	2.0992	.32208
	.381	.5301	-.27563	1.402	1.9508	.29021
	.457	.6361	-.19645	.960	1.3359	.12577

LST SQ FIT TO LOG-LOG EQUATION (R/RC)= 1.178*(X/RC)** -.624 CORRELATION COEFFICIENT= .9119

DEVENS 16OCT73:2LB,HALF-BURIED:GREEN GLASS,1 INCH   CRATER RADIUS(RC)= .719 METERS
PELLET DEPTH OF BURIAL = 2.54CM

FIELD DATA:	----PRESHOT PELLET RANGES-----			----POSTSHOT PELLET RANGES----		
	X METERS	X/RC	LOG10(X/RC)	R METERS	R/RC	LOG10(R/RC)
	.229	.3181	-.49748	28.383	39.4911	1.59650
	.305	.4241	-.37254	16.511	22.3729	1.36122
	.381	.5301	-.27563	4.511	6.2765	.79772
	.457	.6361	-.19645	1.655	2.3028	.36226
	.533	.7422	-.12951	.927	1.2892	.11033

LST SQ FIT TO LOG-LOG EQUATION (R/RC)= .383*(X/RC)** -4.288 CORRELATION COEFFICIENT= .9834

DEVENS 16OCT73:3LB,FULL BURIED:RED ACRYLIC,1 INCH   CRATER RADIUS(RC)= .913 METERS
PELLET DEPTH OF BURIAL = 2.54CM

FIELD DATA:	----PRESHOT PELLET RANGES-----			----POSTSHOT PELLET RANGES----		
	X METERS	X/RC	LOG10(X/RC)	R METERS	R/RC	LOG10(R/RC)
	.381	.4174	-.37949	24.725	27.0851	1.43273
	.457	.5008	-.30031	13.497	14.7846	1.16981
	.533	.5843	-.23336	5.590	6.1235	.78700
	.610	.6678	-.17537	3.280	3.5927	.55542
	.686	.7513	-.12421	1.366	1.4958	.17488
	.762	.8347	-.07846	.972	1.0651	.02739

LST SQ FIT TO LOG-LOG EQUATION (R/RC)= .440*(X/RC)** -4.870 CORRELATION COEFFICIENT= .9946

DEVENS 16OCT73:3LB,FULL BURIED:ORANGE ACRYLIC,2 INCH   CRATER RADIUS(RC)= .913 METERS
PELLET DEPTH OF BURIAL = 5.08CM

FIELD DATA:	----PRESHOT PELLET RANGES-----			----POSTSHOT PELLET RANGES----		
	X METERS	X/RC	LOG10(X/RC)	R METERS	R/RC	LOG10(R/RC)
	.305	.3339	-.47640	17.136	18.7713	1.27349
	.381	.4174	-.37949	7.934	8.6912	.93908
	.457	.5008	-.30031	5.803	6.3573	.80327
	.533	.5843	-.23336	3.658	4.0067	.60278
	.610	.6678	-.17537	1.481	1.6227	.21024
	.686	.7513	-.12421	1.268	1.3890	.14270

LST SQ FIT TO LOG-LOG EQUATION (R/RC)= .554*(X/RC)** -3.263 CORRELATION COEFFICIENT= .9843

Table A2. Preshot and Postshot Distances of Individual Pellets (Cont)

DEVENS 16OCT73:3LB,FULL BURIED:GREEN GLASS,1 INCH   CRATER RADIUS(RC)= .913 METERS
PELLET DEPTH OF BURIAL =   2.54CM

FIELD DATA:	----PRESHOT PELLET RANGES----- X METERS	X/RC	LOG10(X/RC)	----POSTSHOT PELLET RANGES---- R METERS	R/RC	LOG10(R/RC)
	.305	.3339	-.47640	82.082	90.9509	1.95889
	.381	.4174	-.37949	21.190	23.2120	1.36571
	.457	.5008	-.30031	12.143	13.3022	1.12392
	.533	.5843	-.23336	7.541	8.2604	.9170[illegible]
	.610	.6678	-.17537	3.405	3.7295	.57166
	.686	.7513	-.12421	1.301	1.4257	.15403
	.762	.8347	-.07846	1.073	1.1753	.07015

LST SQ FIT TO LOG-LOG EQUATION   (R/RC)=   .493*(X/RC)** -4.701   CORRELATION COEFFICIENT= .9913

DEVENS 16OCT73:4LB,FULL BURIED:RED ACRYLIC,1 INCH   CRATER RADIUS(RC)=1.013 METERS
PELLET DEPTH OF BURIAL =   2.54CM

FIELD DATA:	----PRESHOT PELLET RANGES----- X METERS	X/RC	LOG10(X/RC)	----POSTSHOT PELLET RANGES---- R METERS	R/RC	LOG10(R/RC)
	.305	.3009	-.52153	59.954	59.1935	1.77227
	.457	.4514	-.34544	28.636	28.2726	1.45137
	.533	.5266	-.27849	12.887	12.7234	1.10460
	.610	.6019	-.22050	4.170	4.1168	.61456
	.686	.6771	-.16935	3.085	3.0454	.48365
	.762	.7523	-.12359	1.676	1.6551	.21883
	.838	.8276	-.08220	1.113	1.0984	.04076

LST SQ FIT TO LOG-LOG EQUATION   (R/RC)=   .588*(X/RC)** -4.194   CORRELATION COEFFICIENT= .9732

DEVENS 16OCT73:4LB,FULL BURIED:ORANGE ACRYLIC,2 INCH   CRATER RADIUS(RC)=1.013 METERS
PELLET DEPTH OF BURIAL =   5.08CM

FIELD DATA:	----PRESHOT PELLET RANGES----- X METERS	X/RC	LOG10(X/RC)	----POSTSHOT PELLET RANGES---- R METERS	R/RC	LOG10(R/RC)
	.305	.3009	-.52153	22.064	21.7875	1.33821
	.381	.3762	-.42462	16.374	16.1661	1.20861
	.457	.4514	-.34544	9.077	8.9618	.95239
	.533	.5266	-.27849	8.053	7.9506	.90040
	.610	.6019	-.22050	6.428	6.3467	.80255
	.686	.6771	-.16935	1.768	1.7454	.24190
	.762	.7523	-.12359	1.192	1.1766	.07065

LST SQ FIT TO LOG-LOG EQUATION   (R/RC)=   .737*(X/RC)** -3.093   CORRELATION COEFFICIENT= .9344

DEVENS 16OCT73:4LB,FULL BURIED:GREEN GLASS,1 INCH   CRATER RADIUS(RC)=1.013 METERS
PELLET DEPTH OF BURIAL =   2.54CM

FIELD DATA:	----PRESHOT PELLET RANGES----- X METERS	X/RC	LOG10(X/RC)	----POSTSHOT PELLET RANGES---- R METERS	R/RC	LOG10(R/RC)
	.381	.3762	-.42462	43.983	43.4246	1.63774
	.457	.4514	-.34544	26.953	26.6115	1.42507
	.533	.5266	-.27849	13.777	13.6022	1.13361
	.610	.6019	-.22050	7.202	7.1110	.85193
	.686	.6771	-.16935	4.420	4.3635	.63984
	.762	.7523	-.12359	1.439	1.4204	.15241
	.838	.8276	-.08220	1.073	1.0593	.02501
	.914	.9028	-.04441	1.179	1.1556	.06280

LST SQ FIT TO LOG-LOG EQUATION   (R/RC)=   .565*(X/RC)** -4.685   CORRELATION COEFFICIENT= .9840

DEVENS 16OCT73:2LB,FULL BURIED:RED ACRYLIC,1 INCH(REPRODUC) CRATER RADIUS(RC)= .703 METERS
PELLET DEPTH OF BURIAL =   2.54CM

FIELD DATA:	----PRESHOT PELLET RANGES----- X METERS	X/RC	LOG10(X/RC)	----POSTSHOT PELLET RANGES---- R METERS	R/RC	LOG10(R/RC)
	.152	.2167	-.66408	33.339	47.4122	1.67589
	.229	.3251	-.48799	28.072	39.9220	1.60121
	.305	.4335	-.36305	12.893	18.3355	1.26329
	.381	.5418	-.26614	4.907	6.9788	.84378
	.457	.6502	-.18696	1.189	1.6905	.22802
	.533	.7586	-.12001	1.262	1.7945	.25395

LST SQ FIT TO LOG-LOG EQUATION   (R/RC)=   .872*(X/RC)** -2.980   CORRELATION COEFFICIENT= .9382

DEVENS 16OCT73:2LB,FULL BURIED:ORANGE ACRYLIC,2 INCH(REPROD)CRATER RADIUS(RC)= .703 METERS
PELLET DEPTH OF BURIAL =   5.08CM

FIELD DATA:	----PRESHOT PELLET RANGES----- X METERS	X/RC	LOG10(X/RC)	----POSTSHOT PELLET RANGES---- R METERS	R/RC	LOG10(R/RC)
	.152	.2167	-.66408	11.863	16.8704	1.22713
	.229	.3251	-.48799	3.011	4.2826	.63171
	.305	.4335	-.36305	1.634	2.3234	.36612
	.381	.5418	-.26614	1.411	2.0069	.30253
	.457	.6502	-.18696	.750	1.0663	.02789

LST SQ FIT TO LOG-LOG EQUATION   (R/RC)=   .360*(X/RC)** -2.366   CORRELATION COEFFICIENT= .9015

Table A2. Preshot and Postshot Distances of Individual Pellets (Cont)

~~DEVENS 10/CT73:2LB,FULL BURIED:GREEN GLASS,1 INCH(REPRODUC) CRATER RADIUS(RC)= .703 METERS~~
PELLET DEPTH OF BURIAL = 2.54CM

FIELD DATA:	----PRESHOT PELLET RANGES-----			----POSTSHOT PELLET RANGES----		
	X METERS	X/RC	LOG10(X/RC)	R METERS	R/RC	LOG10(R/RC)
	.229	.3251	-.48799	30.419	43.2596	1.63608
	~~.305~~	~~.4339~~	~~-.36309~~	~~13.991~~	~~19.8398~~	~~1.29753~~
	.381	.5418	-.26614	5.206	7.4036	.86944
	.457	.6502	-.18696	1.603	2.2800	.35794

~~LST SQ~~ FIT TO LOG-LOG EQUATION (R/RC)= .476*(X/RC)** -4.179 CORRELATION COEFFICIENT= .9815

DEVENS 3APRIL74:5LB:SDOB=0.20:RED ACRYLIC, 2 INCH CRATER RADIUS(RC)=1.024 METERS
PELLET DEPTH OF BURIAL = 3.66CM

FIELD DATA:	----PRESHOT PELLET RANGES-----			----POSTSHOT PELLET RANGES----		
	X METERS	X/RC	LOG10(X/RC)	R METERS	R/RC	LOG10(R/RC)
	.305	.2976	-.52634	40.310	39.3601	1.59506
	.381	.3720	-.42943	17.983	17.5595	1.24451
	.457	.4464	-.35025	9.098	8.8839	.94851
	.533	.5208	-.28330	7.199	7.0298	.84694
	.610	.5952	-.22531	5.502	5.3720	.73014
	.686	.6696	-.17416	1.539	1.5030	.17695
	.762	.7440	-.12840	1.204	1.1756	.07026

~~LST SQ FIT TO LOG-LOG EQUATION (R/RC)=~~ .473*(X/RC)** -3.725 CORRELATION COEFFICIENT= .9738

DEVENS 3APRIL74:5LB:SDOB=0.20:YELLOW GLASS, 2INCH CRATER RADIUS(RC)=1.024 METERS
PELLET DEPTH OF BURIAL = 3.66CM

FIELD DATA:	----PRESHOT PELLET RANGES-----			----POSTSHOT PELLET RANGES----		
	X METERS	X/RC	LOG10(X/RC)	R METERS	R/RC	LOG10(R/RC)
	.381	.3720	-.42943	20.955	20.4613	1.31093
	.457	.4464	-.35025	10.982	10.7232	1.03032
	.533	.5208	-.28330	5.081	4.9613	.69560
	.610	.5952	-.22531	3.222	3.1458	.49774
	.686	.6696	-.17416	1.442	1.4077	.14852

LST SQ FIT TO LOG-LOG EQUATION (R/RC)= .270*(X/RC)** -4.464 CORRELATION COEFFICIENT= .9939

DEVENS 3APRIL74:5LB:SDOB=0.20:ORANGE ACRYLIC, 3 INCH CRATER RADIUS(RC)=1.024 METERS
PELLET DEPTH OF BURIAL = 3.66CM

FIELD DATA:	----PRESHOT PELLET RANGES-----			----POSTSHOT PELLET RANGES----		
	X METERS	X/RC	LOG10(X/RC)	R METERS	R/RC	LOG10(R/RC)
	.305	.2978	-.52634	[illegible]	31.4782	1.49798
	.381	.3720	-.42943	[illegible]	16.7798	1.22479
	.457	.4464	-.35025	[illegible]	8.3571	.92206
	.533	.5208	-.28330	3.965	3.8720	.58794
	.610	.5952	-.22531	3.243	3.1667	.50068

~~LST SQ FIT TO LOG-LOG EQUATION (R/RC)= .459*(X/RC)** -3.515 CORRELATION COEFFICIENT= .9925~~

DEVENS 3APRIL74:5LB:SDOB=0.40:RED ACRYLIC: 2 INCH CRATER RADIUS(RC)=1.183 METERS
PELLET DEPTH OF BURIAL = 4.39CM

FIELD DATA:	----PRESHOT PELLET RANGES-----			----POSTSHOT PELLET RANGES----		
	X METERS	X/RC	LOG10(X/RC)	R METERS	R/RC	LOG10(R/RC)
	.305	.2577	-.58883	76.392	64.5954	1.81020
	.381	.3222	-.49192	44.763	37.8505	1.57807
	.457	.3866	-.41274	28.215	23.8582	1.37764
	.533	.4510	-.34579	10.506	8.8840	.94861
	.686	.5799	-.23665	4.496	3.8015	.57996
	.762	.6443	-.19089	3.203	2.7088	.43277
	.838	.7088	-.14950	1.664	1.4072	.14836
	.914	.7732	-.11171	1.433	1.2113	.08327

LST SQ FIT TO LOG-LOG EQUATION (R/RC)= .460*(X/RC)** -3.821 CORRELATION COEFFICIENT= .9933

DEVENS 3APRIL74:5LB:SDOB=0.40:YELLOW GLASS, 2 INCH CRATER RADIUS(RC)=1.183 METERS
PELLET DEPTH OF BURIAL = 4.39CM

FIELD DATA:	----PRESHOT PELLET RANGES-----			----POSTSHOT PELLET RANGES----		
	X METERS	X/RC	LOG10(X/RC)	R METERS	R/RC	LOG10(R/RC)
	.457	.3866	-.41274	36.902	31.2036	1.49420
	.533	.4510	-.34579	23.095	19.5284	1.29067
	.610	.5155	-.28780	9.141	7.7294	.88819
	.686	.5799	-.23665	4.179	3.5335	.54821
	.762	.6443	-.19089	3.147	[illegible]	.42443
	.838	.7088	-.14950	1.951	1.6495	.21735

ST SQ FIT TO LOG-LOG EQUATION (R/RC)= .271*(X/RC)** -5.093 CORRELATION COEFFICIENT= .9921

Table A2. Preshot and Postshot Distances of Individual Pellets (Cont)

DEVENS 3APRIL74;5LB;SDOB=0.40; ORANGE ACRYLIC, 3 INCH   CRATER RADIUS(RC)=1.183 METERS
PELLET DEPTH OF BURIAL = 4.39CM

FIELD DATA:	----PRESHOT PELLET RANGES-----			----POSTSHOT PELLET RANGES----		
	X	X/RC	LOG10(X/RC)	R	R/RC	LOG10(R/RC)
	METERS			METERS		
	.457	.3866	-.41274	29.358	24.8247	1.39488
	.533	.4510	-.34579	9.431	7.9742	.90169
	.610	.5155	-.28780	4.365	3.6907	.56711
	.686	.5799	-.23665	3.652	3.0876	.48963

LST SQ FIT TO LOG-LOG EQUATION (R/RC)= .140*(X/RC)** -5.279 CORRELATION COEFFICIENT= .9718

DEVENS 30APRIL74;5LB;SDOB=0.50; YELLOW GLASS, 2 INCH   CRATER RADIUS(RC)=1.280 METERS
PELLET DEPTH OF BURIAL = 5.72CM

FIELD DATA:	----PRESHOT PELLET RANGES-----			----POSTSHOT PELLET RANGES----		
	X	X/RC	LOG10(X/RC)	R	R/RC	LOG10(R/RC)
	METERS			METERS		
	.457	.3571	-.44716	35.585	27.7976	1.44401
	.610	.4762	-.32222	16.307	12.7381	1.10510
	.686	.5357	-.27107	9.043	7.0643	.84907
	.762	.5952	-.22531	6.757	5.2786	.72252
	.838	.6548	-.18392	4.039	3.1548	.49897
	.914	.7143	-.14613	3.024	2.3619	.37326

LST SQ FIT TO LOG-LOG EQUATION (R/RC)= .737*(X/RC)** -3.626 CORRELATION COEFFICIENT= .9935

DEVENS 6JUNE74;5LB, SDOB=0.50; RED ACRYLIC, 2 INCH   CRATER RADIUS(RC)=1.259 METERS
PELLET DEPTH OF BURIAL = 5.08CM

FIELD DATA:	----PRESHOT PELLET RANGES-----			----POSTSHOT PELLET RANGES----		
	X	X/RC	LOG10(X/RC)	R	R/RC	LOG10(R/RC)
	METERS			METERS		
	.305	.2421	-.61595	23.278	18.4915	1.26697
	.381	.3027	-.51904	17.331	13.7676	1.13886
	.457	.3632	-.43986	12.503	9.9322	.99705
	.533	.4237	-.37291	11.421	9.0726	.95773
	.610	.4843	-.31492	10.257	8.1477	.91104
	.686	.5448	-.26377	8.632	6.8571	.83614
	.762	.6053	-.21801	4.093	3.2518	.51213
	.838	.6659	-.17662	2.774	2.2034	.34309
	.914	.7264	-.13883	1.774	1.4092	.14897

LST SQ FIT TO LOG-LOG EQUATION (R/RC)= 1.134*(X/RC)** -2.164 CORRELATION COEFFICIENT= .9301

DEVENS 6JUNE74;5LB, SDOB=0.50; BLUE GLASS, 2 INCH   CRATER RADIUS(RC)=1.259 METERS
PELLET DEPTH OF BURIAL = 5.08CM

FIELD DATA:	----PRESHOT PELLET RANGES-----			----POSTSHOT PELLET RANGES----		
	X	X/RC	LOG10(X/RC)	R	R/RC	LOG10(R/RC)
	METERS			METERS		
	.305	.2421	-.61595	17.054	13.5472	1.13185
	.381	.3027	-.51904	13.311	10.5738	1.02423
	.457	.3632	-.43986	10.333	8.2082	.91425
	.533	.4237	-.37291	7.778	6.1792	.79093
	.610	.4843	-.31492	5.105	4.0557	.60806
	.686	.5448	-.26377	3.142	2.4964	.39731
	.762	.6053	-.21801	2.042	1.6223	.21012
	.838	.6659	-.17662	1.512	1.2010	.07953
	.914	.7264	-.13883	1.295	1.0291	.01244

LST SQ FIT TO LOG-LOG EQUATION (R/RC)= .516*(X/RC)** -2.534 CORRELATION COEFFICIENT= .9757

DEVENS 6JUNE74; 5LB, SDOB=0.20; BROWN GLASS, 2 INCH   CRATER RADIUS(RC)=1.000 METERS
PELLET DEPTH OF BURIAL = 5.08CM

FIELD DATA:	----PRESHOT PELLET RANGES-----			----POSTSHOT PELLET RANGES----		
	X	X/RC	LOG10(X/RC)	R	R/RC	LOG10(R/RC)
	METERS			METERS		
	.381	.3811	-.41896	31.641	31.6494	1.50037
	.457	.4573	-.33978	13.640	13.6433	1.13492
	.533	.5335	-.27284	4.282	4.2835	.63180
	.610	.6098	-.21484	3.191	3.1921	.50407
	.686	.6860	-.16369	1.341	1.3415	.12758

LST SQ FIT TO LOG-LOG EQUATION (R/RC)= .191*(X/RC)** -5.315 CORRELATION COEFFICIENT= .9917

DEVENS 19JULY74;3/4LB, SDOB=0.00; RED ACRYLIC, 1 INCH   CRATER RADIUS(RC)= .527 METERS
PELLET DEPTH OF BURIAL = [illegible]

FIELD DATA:	----PRESHOT PELLET RANGES-----			----POSTSHOT PELLET RANGES----		
	X	X/RC	LOG10(X/RC)	R	R/RC	LOG10(R/RC)
	METERS			METERS		
	.254	.4821	-.31688	1.865	3.5376	.54871
	.305	.5784	-.23776	.796	1.5087	.17859

LST SQ FIT TO LOG-LOG EQUATION (R/RC)= .117*(X/RC)** -4.678 CORRELATION COEFFICIENT= 1.0000

Table A2. Preshot and Postshot Distances of Individual Pellets (Cont)

```
DEVENS 16JULY74:3/8LB, SCOB=0.0: BROWN GLASS, 1 INCH        CRATER RADIUS(RC)= .527 METERS
PELLET DEPTH OF BURIAL =      2.54CM
                  ----PRESHOT PELLET RANGES-----   ----POSTSHOT PELLET RANGES----
FIELD DATA:        X        X/RC   LOG10(X/RC)        R        R/RC   LOG10(R/RC)
                 METERS                             METERS
                  .254     .4821     -.31688         1.847    3.5029     .54443
                  .305     .5784     -.23776          .860    1.6301     .21220
                  .457     .8674     -.06176          .549    1.0409     .01723

LST SQ FIT TO LOG-LOG EQUATION   (R/RC)=   .735*(X/RC)** -1.907     CORRELATION COEFFICIENT=  .8401


DEVENS 19JULY74:3/8LB, SOOB=0.0: AL, 1 INCH                  CRATER RADIUS(RC)= .527 METERS
PELLET DEPTH OF BURIAL =      2.54CM
                  ----PRESHOT PELLET RANGES-----   ----POSTSHOT PELLET RANGES----
FIELD DATA:        X        X/RC   LOG10(X/RC)        R        R/RC   LOG10(R/RC)
                 METERS                             METERS
                  .254     .4821     -.31688         1.789    3.3931     .53059
                  .305     .5784     -.23776          .576    1.0925     .03842
                  .356     .6748     -.17085          .573    1.0867     .03611

LST SQ FIT TO LOG-LOG EQUATION   (R/RC)=   .230*(X/RC)** -3.472     CORRELATION COEFFICIENT=  .8910


DEVENS 31JULY74:3/8LB, SCOB=0.25: ORANGE ACRYLIC, 1 INCH    CRATER RADIUS(RC)= .622 METERS
PELLET DEPTH OF BURIAL =      2.54CM
                  ----PRESHOT PELLET RANGES-----   ----POSTSHOT PELLET RANGES----
FIELD DATA:        X        X/RC   LOG10(X/RC)        R        R/RC   LOG10(R/RC)
                 METERS                             METERS
                  .152     .2451     -.61066         8.906   14.3235    1.15605
                  .229     .3676     -.43457         3.609    5.8039     .76372
                  .381     .6127     -.21272          .963    1.5490     .19006

LST SQ FIT TO LOG-LOG EQUATION   (R/RC)=   .481*(X/RC)** -2.434     CORRELATION COEFFICIENT=  .9991


DEVENS 31JULY74:3/8LB, SOOB=0.25: AL, 1 INCH                 CRATER RADIUS(RC)= .622 METERS
PELLET DEPTH OF BURIAL =      2.54CM
                  ----PRESHOT PELLET RANGES-----   ----POSTSHOT PELLET RANGES----
FIELD DATA:        X        X/RC   LOG10(X/RC)        R        R/RC   LOG10(R/RC)
                 METERS                             METERS
                  .229     .3676     -.43457         4.173    6.7108     .82677
                  .305     .4902     -.30963         1.454    2.3382     .36889
                  .381     .6127     -.21272         1.012    1.6275     .21151
                  .457     .7353     -.13354          .738    1.1863     .07419

LST SQ FIT TO LOG-LOG EQUATION   (R/RC)=   .499*(X/RC)** -2.465     CORRELATION COEFFICIENT=  .9777


DEVENS 31JULY74:3/8LB, SOOB=0.25: BLUE GLASS, 1 INCH        CRATER RADIUS(RC)= .622 METERS
PELLET DEPTH OF BURIAL =      2.54CM
                  ----PRESHOT PELLET RANGES-----   ----POSTSHOT PELLET RANGES----
FIELD DATA:        X        X/RC   LOG10(X/RC)        R        R/RC   LOG10(R/RC)
                 METERS                             METERS
                  .229     .3676     -.43457         4.377    7.0392     .84752
                  .305     .4902     -.30963         1.606    2.5833     .41218
                  .381     .6127     -.21272          .777    1.2500     .09691

LST SQ FIT TO LOG-LOG EQUATION   (R/RC)=   .235*(X/RC)** -3.388     CORRELATION COEFFICIENT=  .9996


DEVENS 31JULY74:3/8LB, SCOB=0.25: BROWN GLASS, 2 INCH       CRATER RADIUS(RC)= .622 METERS
PELLET DEPTH OF BURIAL =      5.08CM
                  ----PRESHOT PELLET RANGES-----   ----POSTSHOT PELLET RANGES----
FIELD DATA:        X        X/RC   LOG10(X/RC)        R        R/RC   LOG10(R/RC)
                 METERS                             METERS
                  .152     .2451     -.61066         3.206    5.1569     .71239
                  .229     .3676     -.43457         2.409    3.8725     .58800
                  .305     .4902     -.30963         1.161    1.8676     .27129
                  .381     .6127     -.21272          .744    1.1961     .07776

LST SQ FIT TO LOG-LOG EQUATION   (R/RC)=   .592*(X/RC)** -1.634     CORRELATION COEFFICIENT=  .9672


DEVENS 31JULY74:3/8LB, SOOB=0.25: AL, 2 INCH                 CRATER RADIUS(RC)= .622 METERS
PELLET DEPTH OF BURIAL =      5.08CM
                  ----PRESHOT PELLET RANGES-----   ----POSTSHOT PELLET RANGES----
FIELD DATA:        X        X/RC   LOG10(X/RC)        R        R/RC   LOG10(R/RC)
                 METERS                             METERS
                  .152     .2451     -.61066         3.530    5.6765     .75408
                  .229     .3676     -.43457         2.033    3.2696     .51458
                  .305     .4902     -.30963          .853    1.3725     .13753

LST SQ FIT TO LOG-LOG EQUATION   (R/RC)=   .367*(X/RC)** -2.003     CORRELATION COEFFICIENT=  .9746
```

Table A2. Preshot and Postshot Distances of Individual Pellets (Cont)

DEVENS 31JULY74 15/8LB, SDOB=0.25 RED ACRYLIC, 2 INCH — CRATER RADIUS(RC)= .822 METERS
PELLET DEPTH OF BURIAL = 5.08CM

FIELD DATA:	X METERS	X/RC	LOG10(X/RC)	R METERS	R/RC	LOG10(R/RC)
	----PRESHOT PELLET RANGES----			----POSTSHOT PELLET RANGES----		
	.152	.2451	-.61066	3.719	5.9804	.77673
	.229	.3676	-.43457	2.371	3.8137	.58139
	.305	.4902	-.30963	1.173	1.8873	.27583
	.381	.6127	-.21272	.686	1.1029	.04255

LST SQ FIT TO LOG-LOG EQUATION (R/RC)= .491*(X/RC)** -1.857 CORRELATION COEFFICIENT= .9820

DEVENS 10SEPT74 1 LB C4, SDOB=0.00, AL 1 INCH — CRATER RADIUS(RC)= .658 METERS
PELLET DEPTH OF BURIAL = 2.54CM

FIELD DATA:	X METERS	X/RC	LOG10(X/RC)	R METERS	R/RC	LOG10(R/RC)
	----PRESHOT PELLET RANGES----			----POSTSHOT PELLET RANGES----		
	.229	.3472	-.45939	13.692	20.7963	1.31799
	.305	.4630	-.33445	4.697	7.1343	.85335
	.381	.5787	-.23754	2.475	3.7593	.57510
	.457	.6944	-.15836	.991	1.5046	.17743

LST SQ FIT TO LOG-LOG EQUATION (R/RC)= .433*(X/RC)** -3.679 CORRELATION COEFFICIENT= .9959

DEVENS 10SEPT74 1 LB C4, SDOB=0.25, AL 1 INCH — CRATER RADIUS(RC)= .713 METERS
PELLET DEPTH OF BURIAL = 2.54CM

FIELD DATA:	X METERS	X/RC	LOG10(X/RC)	R METERS	R/RC	LOG10(R/RC)
	----PRESHOT PELLET RANGES----			----POSTSHOT PELLET RANGES----		
	.229	.3205	-.49415	35.616	49.9359	1.69841
	.305	.4274	-.36922	13.262	18.5940	1.26937
	.381	.5342	-.27231	5.273	7.3932	.86883
	.457	.6410	-.19312	2.246	3.1496	.49825
	.533	.7479	-.12618	.930	1.3034	.11508

LST SQ FIT TO LOG-LOG EQUATION (R/RC)= .445*(X/RC)** -4.265 CORRELATION COEFFICIENT= .9952

DEVENS 10SEPT74 1 LB C4,SDOB=0.25, AL 3 INCH — CRATER RADIUS(RC)= .713 METERS
PELLET DEPTH OF BURIAL = 7.62CM

FIELD DATA:	X METERS	X/RC	LOG10(X/RC)	R METERS	R/RC	LOG10(R/RC)
	----PRESHOT PELLET RANGES----			----POSTSHOT PELLET RANGES----		
	.152	.2137	-.67025	2.018	2.8291	.45164
	.229	.3205	-.49415	3.667	5.1410	.71105
	.305	.4274	-.36922	1.143	1.6026	.20482
	.381	.5342	-.27231	1.180	1.6538	.21850
	.457	.6410	-.19312	.814	1.1410	.05730

LST SQ FIT TO LOG-LOG EQUATION (R/RC)= .842*(X/RC)** -1.009 CORRELATION COEFFICIENT= .7422

DEVENS 10SEPT74 1 LB C4, SDOB=0.50, AL 1 INCH — CRATER RADIUS(RC)= .841 METERS
PELLET DEPTH OF BURIAL = 2.54CM

FIELD DATA:	X METERS	X/RC	LOG10(X/RC)	R METERS	R/RC	LOG10(R/RC)
	----PRESHOT PELLET RANGES----			----POSTSHOT PELLET RANGES----		
	.229	.2717	-.56585	32.044	38.0906	1.58082
	.305	.3623	-.44091	29.276	34.8007	1.54159
	.381	.4529	-.34400	13.881	16.5000	1.21748
	.457	.5435	-.26482	6.559	7.7971	.89193
	.533	.6341	-.19787	3.286	3.9058	.59171
	.610	.7246	-.13988	1.722	2.0471	.31114
	.686	.8152	-.08873	.978	1.1630	.06560

LST SQ FIT TO LOG-LOG EQUATION (R/RC)= .797*(X/RC)** -3.374 CORRELATION COEFFICIENT= .9882

DEVENS 10SEPT74 1 LB C4, SDOB=0.50, AL 3 INCH — CRATER RADIUS(RC)= .841 METERS
PELLET DEPTH OF BURIAL = 7.62CM

FIELD DATA:	X METERS	X/RC	LOG10(X/RC)	R METERS	R/RC	LOG10(R/RC)
	----PRESHOT PELLET RANGES----			----POSTSHOT PELLET RANGES----		
	.229	.2717	-.56585	12.509	14.8696	1.17230
	.305	.3623	-.44091	9.784	11.6304	1.06560
	.381	.4529	-.34400	4.645	5.5217	.74208
	.457	.5435	-.26482	1.920	2.2826	.35843
	.533	.6341	-.19787	1.317	1.5652	.19457

LST SQ FIT TO LOG-LOG EQUATION (R/RC)= .472*(X/RC)** -2.847 CORRELATION COEFFICIENT= .9881

Table A2. Preshot and Postshot Distances of Individual Pellets (Cont)

DEVENS 10SEPT74: 1 LB C4, SDOB=0.50, AL 4.5 INCH CRATER RADIUS(RC)= .841 METERS
PELLET DEPTH OF BURIAL = 11.43CM

FIELD DATA:	X METERS	X/RC	LOG10(X/RC)	R METERS	R/RC	LOG10(R/RC)
	----PRESHOT PELLET RANGES-----			----POSTSHOT PELLET RANGES----		
	.305	.3623	-.44091	2.481	2.9493	.46972
	.381	.4529	-.34400	1.524	1.8110	.25806
	.457	.5435	-.26482	1.244	1.4783	.16975

LST SQ FIT TO LOG-LOG EQUATION (R/RC)= .498*(X/RC)** -1.721 CORRELATION COEFFICIENT= .9847

DEVENS 10SEPT74: 1 LB C4, SDOB=0.375, AL 1 INCH CRATER RADIUS(RC)= .799 METERS
PELLET DEPTH OF BURIAL = 2.54CM

FIELD DATA:	X METERS	X/RC	LOG10(X/RC)	R METERS	R/RC	LOG10(R/RC)
	----PRESHOT PELLET RANGES-----			----POSTSHOT PELLET RANGES----		
	.229	.2863	-.54324	25.771	32.2710	1.50881
	.305	.3817	-.41830	8.662	10.8473	1.03532
	.381	.4771	-.32139	4.011	5.0229	.70095
	.457	.5725	-.24221	2.350	2.9427	.46875
	.533	.6679	-.17526	1.375	1.7219	.23586

LST SQ FIT TO LOG-LOG EQUATION (R/RC)= .421*(X/RC)** -3.429 CORRELATION COEFFICIENT= .9990

DEVENS 10SEPT74: 1 LB C4, SDOB=0.375, AL 3 INCH CRATER RADIUS(RC)= .799 METERS
PELLET DEPTH OF BURIAL = 7.62CM

FIELD DATA:	X METERS	X/RC	LOG10(X/RC)	R METERS	R/RC	LOG10(R/RC)
	----PRESHOT PELLET RANGES-----			----POSTSHOT PELLET RANGES----		
	.229	.2863	-.54324	2.871	3.5954	.55575
	.305	.3817	-.41830	2.396	3.0000	.47712
	.381	.4771	-.32139	1.753	2.1947	.34137
	.457	.5725	-.24221	1.259	1.5763	.19765

LST SQ FIT TO LOG-LOG EQUATION (R/RC)= .875*(X/RC)** -1.182 CORRELATION COEFFICIENT= .9743

DEVENS 25SEPT74:500 GM C4: SDOB=0.00, AL 1 INCH CRATER RADIUS(RC)= .652 METERS
PELLET DEPTH OF BURIAL = 2.54CM

FIELD DATA:	X METERS	X/RC	LOG10(X/RC)	R METERS	R/RC	LOG10(R/RC)
	----PRESHOT PELLET RANGES-----			----POSTSHOT PELLET RANGES----		
	.229	.3505	-.45535	7.666	11.7523	1.07012
	.305	.4673	-.33041	3.831	5.8738	.76892
	.381	.5841	-.23350	1.881	2.8832	.45987
	.457	.7009	-.15432	.759	1.1636	.06579

LST SQ FIT TO LOG-LOG EQUATION (R/RC)= .629*(X/RC)** -3.267 CORRELATION COEFFICIENT= .9864

DEVENS 25SEPT74: 500 GM C4: SDOB=0.00, AL 2 INCH CRATER RADIUS(RC)= .652 METERS
PELLET DEPTH OF BURIAL = 5.08CM

FIELD DATA:	X METERS	X/RC	LOG10(X/RC)	R METERS	R/RC	LOG10(R/RC)
	----PRESHOT PELLET RANGES-----			----POSTSHOT PELLET RANGES----		
	.229	.3505	-.45535	1.289	1.9766	.29593
	.305	.4673	-.33041	1.317	2.0187	.30507
	.381	.5841	-.23350	.869	1.3318	.12443

LST SQ FIT TO LOG-LOG EQUATION (R/RC)= .983*(X/RC)** -.733 CORRELATION COEFFICIENT= .8013

DEVENS 25SEPT74: 500 GM C4: SDOB=0.25, AL 1 INCH CRATER RADIUS(RC)= .759 METERS
PELLET DEPTH OF BURIAL = 2.54CM

FIELD DATA:	X METERS	X/RC	LOG10(X/RC)	R METERS	R/RC	LOG10(R/RC)
	----PRESHOT PELLET RANGES-----			----POSTSHOT PELLET RANGES----		
	.305	.4016	-.39620	13.655	17.9920	1.25508
	.381	.5020	-.29929	9.080	11.9639	1.07787
	.457	.6024	-.22011	2.861	3.7630	.57322
	.533	.7028	-.15316	1.423	1.8755	.27312

LST SQ FIT TO LOG-LOG EQUATION (R/RC)= .469*(X/RC)** -4.287 CORRELATION COEFFICIENT= .9798

DEVENS 25SEPT74: 500 GM C4: SDOB=0.25, AL 2 INCH CRATER RADIUS(RC)= .759 METERS
PELLET DEPTH OF BURIAL = 5.08CM

FIELD DATA:	X METERS	X/RC	LOG10(X/RC)	R METERS	R/RC	LOG10(R/RC)
	----PRESHOT PELLET RANGES-----			----POSTSHOT PELLET RANGES----		
	.229	.3012	-.52114	9.261	12.2048	1.08651
	.305	.4016	-.39620	7.186	9.4659	.97616
	.381	.5020	-.29929	3.045	4.0120	.60337
	.457	.6024	-.22011	1.987	2.6189	.41809

LST SQ FIT TO LOG-LOG EQUATION (R/RC)= .858*(X/RC)** -2.332 CORRELATION COEFFICIENT= .9607

Table A2. Preshot and Postshot Distances of Individual Pellets (Cont)

DEVENS 25SEPT74: 500 GM C4: SDOB=0.25, AL 3 INCH   CRATER RADIUS(RC)= .759 METERS
PELLET DEPTH OF BURIAL = 7.62CM

FIELD DATA:	X METERS	X/RC	LOG10(X/RC)	R METERS	R/RC	LOG10(R/RC)
	----PRESHOT PELLET RANGES-----			----POSTSHOT PELLET RANGES----		
	.229	.3017	-.52114	1.926	2.5382	.40452
	.305	.4016	-.39620	1.798	2.3695	.37465
	.381	.5020	-.29929	1.591	2.0964	.32147
	.457	.6024	-.22011	.844	1.1124	.04628

LST SQ FIT TO LOG-LOG EQUATION (R/RC)= .804*(X/RC)** -1.063 CORRELATION COEFFICIENT= .8412

DEVENS 25SEPT74: 500 GM C4, SDOB=0.50, AL [illegible] INCH   CRATER RADIUS(RC)= .866 METERS
PELLET DEPTH OF BURIAL = 5.08CM

FIELD DATA:	X METERS	X/RC	LOG10(X/RC)	R METERS	R/RC	LOG10(R/RC)
	----PRESHOT PELLET RANGES-----			----POSTSHOT PELLET RANGES----		
	.305	.3521	-.45332	14.966	17.2887	1.23776
	.381	.4401	-.35641	8.159	9.4261	.97433
	.457	.5282	-.27723	5.435	6.2782	.79783
	.533	.6162	-.21028	2.615	3.0211	.48017
	.610	.7042	-.15229	1.280	1.4789	.16993

LST SQ FIT TO LOG-LOG EQUATION (R/RC)= .538*(X/RC)** -3.453 CORRELATION COEFFICIENT= .9829

DEVENS 25SEPT74: 500 GM C4: SDOB=0.50, AL, 3 INCH   CRATER RADIUS(RC)= .866 METERS
PELLET DEPTH OF BURIAL = 7.62CM

FIELD DATA:	X METERS	X/RC	LOG10(X/RC)	R METERS	R/RC	LOG10(R/RC)
	----PRESHOT PELLET RANGES-----			----POSTSHOT PELLET RANGES----		
	.229	.2641	-.57826	17.160	19.8239	1.29719
	.305	.3521	-.45332	5.754	6.6444	.82245
	.381	.4401	-.35641	5.002	5.7782	.76179
	.457	.5282	-.27723	3.252	3.7570	.57485
	.533	.6162	-.21028	1.637	1.8908	.27666

LST SQ FIT TO LOG-LOG EQUATION (R/RC)= .660*(X/RC)** -2.507 CORRELATION COEFFICIENT= .9761

DEVENS 25SEPT74: 500 GM C4: SDOB=0.50, AL, 4 INCH   CRATER RADIUS(RC)= .866 METERS
PELLET DEPTH OF BURIAL = 10.16CM

FIELD DATA:	X METERS	X/RC	LOG10(X/RC)	R METERS	R/RC	LOG10(R/RC)
	----PRESHOT PELLET RANGES-----			----POSTSHOT PELLET RANGES----		
	.229	.2641	-.57826	8.626	9.9648	.99847
	.305	.3521	-.45332	4.648	5.3697	.72995
	.381	.4401	-.35641	2.972	3.4331	.53569
	.457	.5282	-.27723	2.493	2.8803	.45941
	.533	.6162	-.21028	.890	1.0282	.01206

LST SQ FIT TO LOG-LOG EQUATION (R/RC)= .467*(X/RC)** -2.483 CORRELATION COEFFICIENT= .9901